A NANOENCAPSULATED VISIBLE DYE FOR INTRAOPERATIVE DELINEATION OF BRAIN

TUMOR MARGINS

A Thesis
Presented to
The Academic Faculty

by

Benjamin Thomas Roller

In Partial Fulfillment
of the Requirements for the Degree
Master of Science in Biomedical Engineering in the
School of Biomedical Engineering, College of Engineering

Georgia Institute of Technology
December 2011

A Nanoencapsulated Visible Dye for Intraoperative Delineation of Brain Tumor Margins

Approved by:

Dr. Ravi Bellamkonda, Advisor
School of Biomedical Engineering
Georgia Institute of Technology
Emory University

Dr. Barun Brahma
Pediatric Neurosurgery
Emory University School of Medicine
Children's Healthcare of Atlanta

Dr. Philip Santangelo
School of Biomedical Engineering
Georgia Institute of Technology
Emory University

Date Approved: Sept 22, 2011

ACKNOWLEDGEMENTS

I would like to thank all the people who helped me through my ups and downs through graduate school. First, I would like to thank my parents Treva and Lee Roller for supporting me throughout my life in any endeavor I chose. I would like to thank my brother Shane for always being there for me and offering helpful advice throughout my graduate career.

My undergraduate assistants helped me not only in my lab work but also in life. I would like to thank Karl Guo for his many hours at the cryo-sectioner, staining table, and microscope. I would like to thank Audrey Slutsky for keeping me entertained while we were working together. I would like to thank Anna Olsen for helping me stay organized and laying out the framework for the undergraduate assistants that followed her. I would also like to thank Ravi Patel and Choyce Middleton for their help.

I would like to thank the following people for not only being great colleagues but also for being great friends outside of lab: Dr. Jennifer Munson for keeping me sane in school and out; Alex Ortiz for the many hours of animal surgeries he assisted me with and for the camaraderie outside of lab; Dr. Katie McNeeley for her guidance and allowing me to vent my frustrations; and Clare Gollnick for forcing me to dance any time we went out (even though I secretly wanted to anyway). Special thanks go to Dr. Balakrishna Pai for his many hours of hands on assistance with my project.

I would like to thank my committee members Dr. Barun Brahma and Dr. Philip Santangelo. Barun had a magnificent idea for a tool to help surgeons like himself that led to my MS thesis topic. Without Phil's help, I would not have had microscopic images to prove that my experiments worked.

Finally, and most importantly, I would like to thank my advisor Dr. Ravi Bellamkonda for sticking with me through my emotional, physical, and motivational peaks and valleys. Without his constant support and his want for me to succeed, I would not have been able to accomplish all I did in my graduate career.

TABLE OF CONTENTS

LIST OF TABLES

LIST OF FIGURES

LIST OF SYMBOLS AND ABBREVIATIONS

CNS	Central Nervous System
MRI	Magnetic Resonance Imaging
CT	Computed Tomography
EB	Evans Blue
FDA	Food and Drug Administration
fMRI	Functional Magnetic Resonance Imaging
PET	Positron Emission Tomography
Nano-EB	Nanoparticle Encapsulated Evans Blue
BBB	Blood Brain Barrier
EPR	Enhanced Permeability and Retention
PEG	Polyethylene Glycol
DNA	Deoxyribonucleic Acid
siRNA	Small Interfering Ribonucleic Acid
TERT	Telomerase Reverse Transcriptase
IO	Iron Oxide
PLGA	Poly(lactide-co-glycolide)
PLA	Polylactic Acid
PCL	Poly Caprolactone
MPS	Mononuclear Phagocyte System
RES	Reticuloendothelial System
DPPC	1,2 –Dipalmitoyl-sn-glycero-3-phosphocholine
MPEG-2000-DSPE	N-(carbonyl-methoxypolyethyleneglycol-2000)-1,2--distearoyl-sn-glycero-3-phosphoethanolamine
PBS	Phosphate Buffered Saline

MWCO	Molecular Weight Cut-off
DLS	Dynamic Light Scattering
β-DPH-HPC	2-(3-(diphenylhexatrienyl)propanoyl)-1-hexadecanoyl- -*sn*-glycero-3-phosphocholine
FBS	Fetal Bovine Serum
GFP	Green Fluorescent Protein
DAPI	4',6-diamidino-2-phenylindole

SUMMARY

Brain and central nervous cancer presents a significant clinical burden, accounting for 2.4% of all cancer deaths. High grade glioma is particularly deadly, with 5 year survival times of 35% or less. Traditional treatment includes tumor resection followed by radiation therapy or chemotherapy. Aggressive resection is essential in order to prolong patient life. In fact, several studies have shown that life expectancy increases with increased extent of resection. Extent of resection is burdened by the fact that surgeons must be careful not to remove functional brain tissue.

Resection is incomplete more often than not due to lack of visual cues for the surgeon. He must rely on tactile sensation to distinguish tumor from healthy tissue. Methods such as intraoperative MRI and CT exist, but these require expensive equipment and special training that is not available in all surgical environments. Some laboratories have proposed small molecule dyes to solve this problem, but these are insufficient when used in an invasive tumor model. It was the goal of this research to provide an objective cue in the form of a nanoencapsulated visible dye without the need for additional equipment of changes to the surgery process itself other than injection of the dye.

We hypothesized that the nanocarrier would allow staining of the tumor through passive targeting by taking advantage of the enhanced permeability and retention effect. Once the nanocarriers have reached the desired target, they would not diffuse out into healthy tissue due to their large size compared to small molecule dyes, which readily diffuse out and stain healthy tissue.

To test this hypothesis, we prepared and characterized a liposomal nanocarrier encapsulating Evans blue dye. The nanocarrier was tested for safety in vitro and in vivo,

then used to delineate tumor margins in an invasive rat glioma model in vivo. Microscopic analysis was then conducted to ensure only tumor tissue was stained by the nanocarrier. This thesis presents a successful method of tumor border delineation to provide surgeons with positive visual cues without the need for changes in surgical environment or techniques.

CHAPTER 1

INTRODUCTION

1.1 Statement of Problem

Malignant brain cancer, specifically glioma, is a deadly disease with generally poor treatment outcomes. There were approximately 22,000 new cases of brain and central nervous system (CNS) cancers in adults in 2008, resulting in a five year survival rate of 35%. Roughly 20% of these cases were glioma with even poorer prognosis [1]. Malignant glioma is currently the second most deadly cancer in middle aged adults and adolescents [2]. Successful treatment of glioma is difficult due to its rapid growth rate and tendency to invade into healthy tissue.

Currently, aggressive surgical resection is the primary method used to extend survival for patients suffering from high grade glioma [3-7]. Even with treatment, prognosis is poor, resulting in a mean survival time as low as 11 to 14 months [8]. However, patient life expectancy increases with an increase in extent of resection [5, 8]. Concomitantly, minimizing removal of healthy neural tissue is critical to ensure quality of life. As a consequence, total and complete surgical resection of tumors is rare, and a vast majority of brain tumors recur, often in close proximity to the resection site [9, 10].

A major impediment to achieving greater accuracy in tumor resection stems from the absence of clear visual cues demarcating the tumor margin and poor tools to enable accurate demarcation of tumor margins. Therefore, neurosurgeons currently rely on subjective criteria, such as tactile feedback and slight discoloration, to assess whether tissue is healthy or tumor. Presurgical magnetic resonance imaging (MRI) or computed tomography (CT) can provide relevant information to plan the surgical procedure, but

1

does not provide real-time information during resection. Intraoperative histology can provide surgeons with information about the margins, but this method can be time consuming and can only assess whether tissue is healthy or tumor after it is removed from the patient. Intraoperative CT or MRI are possible alternatives, providing non-invasive information about extent of remaining tumor, but are expensive and special training is often needed, so these techniques are only available in more advanced surgical environments. Fluorescent probes that stain tumors have been reported but they require special equipment for excitation and detection, as well as low light conditions, neither of which is optimal in a surgical environment [11-15]. Thus, a method to demarcate tumor margins without a significant change to surgical conditions is desired. Demarcation of the tumor margin will allow more accurate and complete removal of tumor tissue, conceivably leading to extended survival times for patients.

1.2 Hypothesis

A method to demarcate tumor margins without a significant change to surgical conditions is desired to increase efficiency of resection. Ozawa, Orringer, and their respective colleagues have suggested the use of a freely injected visible dye to address this challenge [16, 17]. This is an elegantly simple solution; however, the demarcation is transient so such a dye must be injected several times during the course of the surgical procedure. More importantly, the technique stains healthy tissue in more invasive tumors, where a real need for demarcation is present. A non-invasive tumor such as the 9L line used by Ozawa and others merely "pushes" healthy tissue out of the way as it grows so the tumor margin is already fairly distinguished; the tumor extracellular space and vasculature do not interact with the healthy tissue [18]. Clearly, this is not the case with

most invasive tumors; diffusion through extracellular space would cause staining of healthy tissue, as seen in our experiments with injections of Evans blue (EB) dye dissolved in sterile saline.

Previous studies by our lab have shown that a nanoencapsulated x-ray contrast agent will passively but selectively accumulate at the periphery of the tumor [19]. Due to their relatively large size (~100-200 nm), these nanoparticles mark the margin stably without diffusing away, moving no more than 50 µm from the vessel from which they exited [20]. Further, liposomal nanocarriers are Food and Drug Administration (FDA) approved for use in cancer for delivery of chemotherapeutics, such as Doxil®, which yields predictable circulation times and biodistribution, as well as reduces systemic toxicity [21-23]. Our **hypothesis** is that a nanoencapsulated dye would overcome the problem with diffusion seen with small molecule dyes and stably delineate the tumor margin since nano-sized particles do not readily diffuse through tissue, even in an invasive cancer model.

1.3 Objectives

The purpose of the work in this thesis is to use a nanocarrier encapsulated visible dye to provide accurate visual cues for the surgeon to intraoperatively delineate tumor margins without the need for MRI, fluorescence, or other equipment. Emphasis is placed on not only efficacy, but also safety.

To meet this goal, the following objectives were set:

1. Design, fabricate, and characterize a nanocarrier that encapsulates a visible dye.
2. Demonstrate safety in vitro as well as in vivo.
3. Demonstrate ability of the nanocarrier to demarcate the border of an invasive tumor in vivo.

3

CHAPTER 2

RELEVANT BACKGROUND

2.1 Cancers of the Brain and Central Nervous System

The most common cancers of the brain arise from mutations in the support cells of the brain, the glia, and are thus termed glioma. The most common subtype is astrocytoma, while oligodenrocytomas are less common and ependymomas the least common [24, 25]. Glioma is an aggressive and deadly disease. There are approxiately 20,500 new cases of glioma reported and 12,500 deaths caused by glioma each year. While glioma account for only about 1.4% of all cancers, they are responsible for 2.4% of all cancer deaths [26]. Glioma are graded from Grade I (least malignant) to Grade IV (most malignant) [27, 28].

Grade I tumors (ex. pilocytic astrocytoma) are slow to proliferate and are not migratory or invasive, making surgical resection simple compared to advanced grades. In fact, resection is often all that is needed to cure the patient of this malady. Grade II tumors (ex. astrocytoma) proliferate slowly, similar to Grade I, but are infiltrative. Thus, resection may not remove all cancerous cells and recurrence is common after resection. It is not unusual for this type of tumor to progress to a Grade III lesion (ex. anaplastic astrocytoma), which is characterized by malignancy, rapid proliferation, and nuclear atypia. Resection of these tumors is often followed by radiation and/or chemotherapy. Grade IV tumors (ex. glioblastoma) present the greatest challenge in clinic and are typically fatal, often taking the lives of their hosts within a year. These highly malignant lesions are characterized by rapid proliferation and large amounts of invasion. Tumors of this grade typically have the ability to rapidly recruit and produce their own vasculature.

4

Tumor growth is so rapid, however, that new vasculature is often not sufficient enough to supply blood to the entire tumor; thus, necrotic regions are common in this type of lesion. Invasion and infiltration of surrounding tissue often results in satellite tumors in other regions of the brain and central nervous system [28, 29].

Grade I glioma rarely progress to stage II-IV and thus prognosis is generally good; full recovery is not uncommon [30]. Grade II glioma are less malignant and easier to treat than higher grade tumors; therefore, they generally have better prognoses with median survival times of 5-8 years [28, 31]. Grade III gliomas are more malignant than the lower grade tumors, and thus have a lower median survival time of 3 years. The most deadly are the Grade IV glioma with median survival rates of less than a year. Despite advances in cancer treatment and therapy, glioblastoma and other highly malignant brain tumors result in death more often than not, with 5 year survival rates of only 35% and lower [1]. Some strategies for diagnosis and treatment of brain and central nervous tumors are discussed below.

2.2 Diagnosis and Treatment of Brain Cancer

Symptoms of glioma are highly varied according to the position, size, and invasive characteristics of the particular tumor. Symptoms can include seizures, confusion, memory loss, personality change, other neurological deficits, and headaches, though headaches experienced by patients are often indistinguishable from normal tension headaches [25]. Patients that present these symptoms generally undergo brain imaging for diagnosis.

CT and MRI are the most common modalities for diagnosing brain tumors. CT is less expensive and often more readily available, but may not always accurately diagnose

5

tumor due to lack of contrast [32]. MRI is much more sensitive and more accurately diagnoses tumor. On T1 weighted MRI, glioma presents as a heterogeneously enhancing region surrounded by highly contrasting edema [25]. Functional MRI (fMRI) provides information on location of vital function which can aid in surgical planning. Other methods that provide additional information about a lesion after initial diagnosis aid in treatment.

Metabolic activity of a tumor can provide insight on type and grade of a tumor without biopsy, as well as help monitor response to therapy [33]. Positron Emission Tomography (PET) can be used to monitor metabolic activity using contrast agents such as ^{18}F-fluorodeoxyglucose, ^{18}F-fluoro-L-thymidine, ^{11}C-methionine, and 3,4-dihydroxy-6-^{18}F-fluoro-L-phenylalanine. Treatment response can also be monitored indirectly using diffusion-weighted imaging and diffusion tensor imaging, which provide insight into tumor perfusion and vessel permeability [34]. This information can be used to infer tumor grade, though biopsy and histological analysis is needed to confirm grade.

Grading of a specific tumor influences the approach taken to combat it in clinic. Other factors include patient information and overall health, tumor location, extent of contrast enhancement (MRI or CT), proliferation indices, genetic alterations, and previous surgical or therapeutic interventions [28]. Low grade tumors are often met with resection alone, while higher grade tumors get a combination of resection and radiotherapy or chemotherapy. Resection reduces so called "mass effect", or complications associated with increased intracranial pressure due to the mass and volume of the bulk tumor. Radiation therapy or chemotherapy aim to eliminate or reduce the

6

number of cells that were either missed during resection or had already invaded beyond the tumor margin and into healthy tissue, where resection is not possible.

Resection of glioma remains the primary means of treatment to extend patient life [3-7, 25]. In fact, studies have shown that more complete resection of tumor correlates to greater extension of patient life [5, 8]. Complete resection is difficult, however, due to the fact that a surgeon must be careful not to remove functional tissue.

Resection of brain tumors differs significantly from treatment of tumors in less essential organs and tissue. For example, in breast cancer a surgeon has the option to remove the entire breast to ensure every malignant cell is removed without compromising health of the individual. Though this may cause cosmetic issues, it is not essential to the life of the patient. With brain tumors, however, you are limited in the amount of excess tissue you can remove. One must be careful not to remove healthy, functional brain tissue while maximizing extent of resection. This is often difficult due to lack of objective criteria to distinguish healthy from tumor tissue.

Currently, surgeons rely on tactile feedback and very slight discoloration of tumor tissue to distinguish it from healthy tissue. Preoperative CT, MRI, and fMRI allow planning of surgery, but once surgery has begun the surgeon must rely on his experience to distinguish healthy from tumor tissue. Surgeons use suction to remove tumor tissue, which is often less dense and softer than healthy tissue. Current "intraoperative" methods of tumor detection require surgery to pause so that the tissue can be assessed.

Intraoperative MRI and CT are methods used to assess location of malignant tissue during surgery. Though useful in distinguishing tumor tissue from healthy, surgery must be halted for scans to be taken. Also, these methods require expensive equipment

7

and highly trained surgeons and support staff to operate effectively. Thus, this technology is cost prohibitive and only available in a few surgical environments. Another method currently used to assess malignancy of tissue during surgery is intraoperative histology. A surgeon removes a suspect sample from the patient and histology is performed on the sample. The sample is then analyzed by an experienced pathologist to determine whether the tissue is cancer or healthy. There are a few flaws to this approach. First, it is time consuming and surgery must be halted to wait for the results. Second, and more importantly, this method only tells you if you have removed healthy tissue after it has been removed. Thus, the method may not prevent a surgeon from removing functional tissue.

After resection, it is common to follow up with radiation therapy or chemotherapy to get rid of any remnant cancer cells. These cells could have been left behind due to incomplete resection or could have invaded away from the bulk tumor into healthy tissue. Radiotherapy is commonly used for adults, but used much less frequently in children to avoid developmental complications [32]. Radiation treatment after resection has been shown to increase survival in patients with Grade IV glioma up to 9 months [35, 36]. Radiotherapy must be used with caution in elderly patients; reduced doses and frequency of treatment are often required. Thus, median survival is only marginally increased from 16.9 weeks to 29.1 weeks [37]. Even with radiation treatment, up to 90% of tumors recur at the original tumor site [38], so other methods must be explored to increase survival.

Chemotherapy is becoming more common for treatment of glioma with new advances in available drugs and delivery methods. Common chemotherapeutic drugs include temozolomide injections and carmustine delivered in the form of Gliadel Wafers.

Temozolomide treatment after resection shows moderate increases in survival time, and concomitant radiotherapy and temozolomide treatment after resection results in a 2 year survival rate increase of approximately 16% compared to radiation alone [36]. Use of Gliadel Wafers, manufactured by MGI Pharma, leads to increased survival of 2-3 months [39]. However, these increases in survival are still marginal so better treatment regiments are needed to extend patient life.

Though resection is often supplemented with radiation therapy or chemotherapy, resection is still the primary, gold standard treatment to increase patient survival time. It has been shown that increasing completeness of resection at the primary tumor site could lead to increased survival [5, 8]. However, resection is complicated by the fact that tumor tissue is often similar in texture and color to healthy tissue. Since surgeons must remove as much of the bulk tumor as possible while preserving healthy tissue, there is a clinical need for objective means of distinguishing tumor from healthy tissue. This could be achieved by staining tumors in vivo to provide visual contrast between tumor and healthy tissue. Some recent work in staining tumors to provide objective criteria is discussed below.

2.3 Recent Work in In Vivo Tumor Staining

There have been many attempts to stain tumors in vivo using small molecule visible and/or fluorescent dyes. Initially, use of vital dyes for tumor resection aimed at tracing lymph drainage to indicate sentinel lymph nodes (reviewed by Bostick and Giuliano [40]). Tumors such as melanoma and some forms of breast tumors are known to migrate or invade into lymph nodes, where they go on to metastasize into other tissues in the body. For this reason, sentinel lymph nodes are often removed during tumor

9

resection. Morton et al attempted to stain and detect sentinel lymph nodes using various dyes, including methylene blue, isosulfan blue, patent blue-V, cyalume, and fluourescein [41]. Many of these dyes, when injected, diffused throughout the tissue making lymph node detection impossible. However, 2 dyes, patent blue-V and isosulfan blue, remained in the lymphatics without diffusing throughout the tissue, allowing tracking of sentinel lymph nodes.

Use of the previously mentioned dyes in clinic allowed surgeons to precisely remove sentinel lymph nodes in melanoma and breast cancers, as well as other solid tumors where metastasis through lymph vessels was suspected [41-44]. Tanaka et al sought to use fluorescent tags to achieve the same goal with greater sensitivity [45]. Indocyanine green, an FDA approved dye that fluoresces in the near infrared range, was adsorbed to human serum albumin and injected peri-tumorally. The dye then travelled through the lymph to sentinel lymph nodes and was detected using fluorescent microscopes. Though more sensitive than methods using visible dyes, this method requires introduction of fluorescence activating and detecting equipment, as well as alteration of the lighting in the surgical environment. Typical halogen lights used in modern surgical settings emit not only visible light but light in the near infrared range as well. Therefore, halogen lights cannot be used without introducing interfering infrared radiation.

Since the vasculature of brain tumors have compromised blood brain barrier (BBB) and endothelial cell linings, small molecules and nano-scale particles extravasate into tumor intracellular space. Once the molecules extravasate, they do not readily leave the extracellular space due to a disorganized or non-existent lymph drainage system in

10

the tumor. This phenomenon is known as the enhanced permeability and retention (EPR) effect [46, 47]. The EPR effect allows intravenously injected drugs and contrast agents to passively target and accumulate in tumors. This method was and is still used by researchers to deliver agents that dye tumors in vivo.

The first attempts to stain tumors in vivo were done using fluorescent compounds. Fluorescein was used early on, but requires ultraviolet radiation to detect and undergoes rapid clearance due to it being a small molecule dye [48]. Laser activated dyes were explored next, but these dyes did not stain tumors sufficiently to mark the margins with enough precision and, again, rapid clearance was a problem [49, 50]. Indocyanine green was explored with some success by Hansen and colleagues [51]. Tumor bearing animals received indocyanine green intravenously. Tumors were visualized using near infrared equipment and resection was performed based on tissue fluorescence. However, residual tumor was discovered after resection.

Other attempts at marking tumors used Cy5.5 dye conjugated to iron oxide particles [12]. This allowed MRI contrast as well as fluorescence contrast, allowing both preoperative and intraoperative detection of tumors. Nguyen and collegues used similar Cy5 dye conjugated to cell penetrating peptides to fluorescently stain tumors [15]. Pham and colleagues went as far as to synthesize a water-soluble near infrared dye for conjugation to nanoparticles and use for tumor detection [13]. This dye was more fluorescent than previously available dyes so detection of tumor was more sensitive. Qian et al addressed the sensitivity issue by employing Raman spectroscopy to detect their tumor targeting agent [52].

Though all of these methods were effective to an extent, they all required specially adapted equipment such as fluorescence excitation lasers or diodes and detection equipment, as well as special lighting conditions. It would be beneficial if one could employ a means of tumor detection that did not require these changes to the surgical environment. Thus, the next logical step in tumor staining was attempting to stain them using visible dyes.

One of the first attempts to stain brain tumors with a visible dye was performed by Ozawa and colleagues [16]. Bromophenol blue was injected intravenously into animals bearing 9L glioma tumors. While the injections did result in tumor staining with no adverse effects to the animal, there were some problems. The dye was rapidly cleared from the tumor, so extent of staining was highly temporally dependent. The more vascularized border region of the tumor is the first area of the tumor to clear small molecule dyes. Thus, in the bromophenol blue experiments, the margins of the tumors were only distinguishable momentarily. Orringer and colleagues performed similar experiments using Coomassie blue and a "window" implanted into the skull to view the staining in real time [17]. These experiments showed similar results to those using bromophenol blue. But there is one fatal flaw to these approaches.

Attempts to stain tumors with small molecule dyes thus far have used non-invasive tumor models such as rat 9L glioma. These tumors do not interact with neighboring tissue; they merely push healthy tissue out of the way as they grow [18]. Thus, they are inherently delineated and do not accurately mimic those tumor seen in clinic. Clinically relevant tumor models invade neighboring tissue and degrade extracellular matrix. This blurs the line between healthy and malignant tissue and allows

12

small molecule dyes to diffuse into healthy tissues (data presented in results section). Encapsulation of a small molecule dye in a nano-scale particle could possibly be used to solve this problem.

2.4 Nanocarriers for Delivery of Chemotherapeutic and Contrast Agents to Tumors

2.4.1 Advantages of Nanocarriers

Nanoparticles are structures that have at least 1 nano-scale dimension (1 to several 100 nm). In nano-medicine, these particles have been employed to deliver chemotherapeutic drugs for treatment of cancer and contrast agents for medical imaging. Nanoparticles decrease systemic exposure to the injected agent compared to freely injected compounds, which often leads to decreased systemic toxicity and lessens other adverse effects. Nanoparticles allow passive targeting to areas of interest with compromised, leaky vasculature, such as that present in tumors.

Passive targeting of tumors by nanoparticles occurs via the phenomenon termed the enhanced permeability and retention (EPR) effect [46, 47]. Rapidly growing tumor lesions require rapid angiogenesis to sustain their high rate of metabolic activity. Vessels that grow in these lesions grow so rapidly and in such a disorganized manner that tumor vasculature is often unorganized and leaky. Leaky vasculature results from the rapid and insufficient proliferation of endothelial cells, which line blood vessels, and pericytes, which help to maintain impermeable sections of the vasculature such as the BBB. This results in blood vessel fenestrations on the order of several hundred nanometers compared to the 5-10 nm present in healthy tissue [53]. Nanoparticles are free to leak through these fenestrations into the tumor interstitium, but are too large to leak into healthy tissue [54, 55]; the result is lowered systemic exposure to the encapsulated

13

molecules. Retention of nanoparticles occurs due to the fact that tumor tissue often has compromised or insufficient lymphatic drainage [46]. Rapid proliferation of tumor cells results in pinching off of lymph vessels so drainage cannot occur. The combination of the leaky vasculature and poor lymph drainage is responsible for the EPR effect. Nanoparticles not only help in getting the molecules of interest to the tumor, but ensure that they do not diffuse out of the target into healthy tissue.

Freely injected small molecule dyes tend to diffuse rapidly in invasive tumors, often resulting in healthy tissue staining. One way to overcome the problem of diffusion is to encapsulate the small molecule dye in a nanoparticle. Nanoparticles are small enough to still accumulate in tumors due to the EPR effect, but they are large enough that they do not readily diffuse through tissue. In fact, nanoparticles that extravasate into tumors through leaky vasculature often remain within 50 µm of the vessel through which they exited [20].

Several types of nanoparticles have been developed that successfully encapsulate and deliver small molecule drugs and contrast agents to tumors, including dendrimers, carbon nanotubes, metallic nanoparticles, polymeric nanoparticles, and liposomes.

2.4.2 Dendrimers

Dendrimers are globular or spherical multi-branched nanoparticles that resemble the branches of a tree; they are composed of synthetic polymers such as polyamidoamine, polyethylene oxide, glycerol, and succinic acid, or natural polymers, such as amino acids, nucleotides, or sugars [56, 57]. Having many branches increases the surface area for conjugation of targeting molecules, chemotherapeutic agents and other drugs, and contrast agents. Dendrimers have been used to deliver chemotherapeutics and contrast

14

agents, as well as for photodynamic therapy and even gene therapy for treatment of cancer [57].

Dendrimers are versatile structures that enable conjugation of targeting moieties and protective surface modifications. Drugs and other small molecules can be encapsulated via covalent binding to the branches or can be weakly associated with the core. The core can accommodate hydrophobic or hydrophilic drugs depending on the surface chemistry of the core itself; molecules can be held by hydrophobic or hydrophilic interaction, as well as electrostatic interactions and hydrogen bonding [58]. However, binding through these methods result in particles that leak their contents rather quickly in solution, as seen when researchers attempted to encapsulate doxorubicin in this manner [59]. After drug loading, each dendrimer encapsulated an average of only 6.5 molecules of doxorubicin. When placed in isotonic solution, these molecules quickly dissociated from the dendrimer core. Other chemotherapeutic dendrimers include those bound to paclitaxel [60] and methotrexate [61]. Both of these examples, in addition to a chemotherapeutic, also contained the targeting small molecule folate. Folate receptor is often overexpressed on cancer cell surfaces enabling targeting via the folate molecule. Therapeutic effect was greater in each case than treatment with the free molecule version of their respective chemotherapeutic.

Dendrimers have been used as delivery methods for contrast agents as well. Olson and colleagues conjugated gadolinium chelates to dendrimers containing cell penetrating peptides to monitor the activity of proteases in vivo via MRI [62]. Another dendrimer was designed by Konda and colleagues [63]. The dendrimer contained both folate and a gadolinium chelate and allowed visualization of ovarian tumors in animals.

15

Fluorochromes have also been conjugated to dendrimers to enable fluorescence monitoring of physiological activity of cells in tumors [57].

The major drawback to dendrimers for use in our research is that in order to stably encapsulate drugs and contrast agents, one must covalently bind the agent to the polymer. This not only makes synthesis more difficult, but also results in a decreased total payload compared to other nanoparticles such as liposomes or polymeric nanoparticles with aqueous cores (discussed below). Also, when dealing with dyes, slight alteration to the structure through binding alters the resonance of the atoms within the molecule. Altering the resonance can change the wavelengths of visible light the molecule absorbs and reflects, thus changing the color of the dye. This not desirable in our application since we want to maintain the deep, dark blue of the Evans blue molecule we used to dye the tumor.

2.4.3 Carbon Nanotubes

Carbon nanotubes are single- or multi-walled cylindrical cage structures made up of benzene rings. Carbon nanotubes are thus extremely hydrophobic so surface modification, such as coating with PEG, is required to make them soluble in aqueous solutions. They have been used to encapsulate chemotherapeutics, target tumors, and deliver DNA or siRNA to cancer cells.

Carbon nanotubes have been used to encapsulate chemotherapeutics such as doxorubicin [64], resulting in successful treatment of tumors. Doxorubicin was also bound to PEG coated nanotubes in a pH dependent manner [65]. The binding was stable at physiological pH, but allowed release of the drug in acidic conditions like those present in endosomes or lysosomes of cells. When treated with these nanoparticles,

16

MCF-7 breast cancer cells and U87MG human glioblastoma cells showed high levels of cell death in vitro.

Nanotubes targeted with RGD peptides were used to target integrin positive tumors in a mouse model using the U87MG human glioblastoma cell line. Nanotubes were coated with PEG molecules, which were then bound with RGD peptide [66]. MicroPET images of tumor bearing mice demonstrated selective delivery of targeted nanotubes to the tumor site.

Carbon nanotubes have been used effectively to deliver DNA in vivo. Folic acid coated nanotubes were used to deliver small DNA segments into folate receptor over-expressing HeLa cells [67]. The cells were then exposed to pulses of NIR radiation to cause endosomal release of the DNA nanotubes, which allowed DNA to then enter the nucleus of the cells. Minimal toxicity of the nanotubes was observed, but the long term effects of carbon nanotubes have yet to be discovered.

Carbon nanotubes have been used to deliver siRNA to silence telomerase reverse transcriptase (TERT) function in a murine tumor model [68]. Nanotubes with the anti TERT siRNA induced tumor cell growth arrest, resulting in longer survival times for nude mice inoculated with HeLa tumors.

In vivo use outside of a laboratory environment relies on the further investigation of the long terms effects of carbon nanotubes in the body. Little is known about their long term fate after injection and chronic complications that may develop.

2.4.4 Metallic Nanoparticles

Nanoparticles made of metals such as gold and iron can be used to encapsulate small molecules. Gold nanoparticles can take the shape of spheres, rods, and cubes or

17

cages. Generally, the only way to "encapsulate" molecules using gold is to attach the desired molecule to the surface of the particle either covalently or through hydrophobic interactions. This limits their utility as delivery vectors. Though gold nanoparticles can be used to encapsulate molecules, their primary use in experimental cancer treatment methods is tumor ablation or activation of thermosensitive nanocarriers.

Gold nano-rods and shells can be tuned via alteration of dimensional ratios to generate heat in response to stimulation by different frequencies of light [69, 70]. The most useful of these are rods and shells that respond to near infrared radiation. Near infrared light can penetrate soft tissue up to 10 cm with little loss of energy due to minimal absorption and scattering by intrinsic pigments [71]. Thus, it can be used to stimulate gold nanoparticles to generate local hyperthermia of several degrees which could be utilized for initiating triggered release of encapsulated agents from thermosensitive nanoparticles. Paasonen et al. has provided a proof of concept of this method [69]. Gold nanoparticles were incorporated into calcein loaded liposomes. The liposomes were stable at 37°C, and upon illumination with near infrared light, localized heating occurred resulting in calcein release.

The use of thermosensitive nanoparticles in conjunction with gold nanorods has been shown to improve efficacy of nanocarrier delivered doxorubicin in combating cancer. Agarwal and colleagues used this method to treat U87 tumors in mice [72]. Treatment with thermosensitive liposomes triggered by gold nanorod heating caused greater exposure of the cells of the tumor to the doxorubicin encapsulated, thus creating more tumor cell death and longer survival times in mice compared to doxorubicin liposome treatment alone.

18

Iron oxide (IO) nanoparticles are similar to gold nanoparticles in that they require conjugation of the desired molecules to the surface of the particles. Though this allows the option of transporting small molecule dyes and drugs, IO particles are generally used as MRI imaging contrast agents; they appear as hypointense regions on MRI images [73]. Not only have IO nanoparticles been used to visualize tumors, but they have also been used to track specific cell types such as stem cells by adhering appropriate targeting molecules [74].

2.4.5 Polymeric Nanoparticles

Polymeric nanoparticles are composed of natural or synthetic polymers such as poly(lactide-co-glycolide) (PLGA), polylactic acid (PLA), poly caprolactone (PCL), and chitosan. The most common polymer nanoparticles are nanospheres, which are solid, or nanocapsules, which contain a hollow or aqueous central core [75]. Both are well suited for encapsulation of small molecules. Depending on the chemistry of the nanoparticle, it can be used to encapsulate hydrophilic or hydrophobic molecules. Polymeric nanoparticles have even been used to encapsulate proteins and nucleic acids [76]. Surface modifications allow attachment of targeting moieties, such as RGD or folate, or protection from the MPS by attaching PEG chains (discussed below).

One advantage of polymeric nanoparticles is that one can tune the rate of degradation of the particle by varying the ratio of biodegradable polymers. However, a major disadvantage is that many of the manufacturing methods for polymer nanoparticles require use of toxic solvents. These must be extensively rinsed and removed before use in vivo. Though promising as molecule delivery agents, there are no polymeric

19

nanoparticles currently approved by the FDA for use in treatment of cancer, though there are several in clinical trials at time of writing [77].

2.4.6 Liposomes

Liposomes are spherical nanoparticles made up of phospholipids in a lipid bilayer, similar to that of cells. This makes them highly biocompatible. In fact, almost all of the nanoparticles that are FDA approved for use in humans are liposomal formulations. Liposomes can be used to encapsulate large amounts of hydrophilic drugs in the aqueous core or hydrophobic drugs in the lipid bilayer. Liposomes are by no means cutting edge technology, having been first developed in the 1960's [78], but their utility still remains. Since their inception, liposomes have been used extensively both in clinic and in laboratories to encapsulate drugs and contrast agents.

Some of the first nanoscale therapeutics approved for human use were liposomal nanoparticles that encapsulate cytotoxic anthracycline-derived antitumor drugs. Myocet™, liposomal doxorubicin, and DaunoXome™, liposomal daunorubicin, are indicated for use as anticancer agents. Packaging chemotherapeutic drugs in liposome vessels allows for accumulation in the tumor while reducing the deadly cardiotoxicity associated with freely delivered anthracyclines. Newer formulations of these drugs, like Doxil™, are coated with polyethylene glycol (PEG) to protect them from clearance by the MPS thereby prolonging circulation time in the bloodstream. So-called sterically stabilized or "Stealth" liposomes are able to evade opsonization and MPS clearance, which is discussed in the next section.

Contrast agents have also been encapsulated in liposomes. In studies conducted by Karathanasis el al., an iodine contrast agent (Visipaque 320, GE Healthcare,

20

Milwaukee, WI) was encapsulated in 100 nm liposomes and delivered to rats that were inoculated with 13762 MAT B III breast tumors. Mammography was performed on a clinical mammography system (Senographe 2000D, GE Healthcare) for three consecutive days. Images were used to calculate the amount of enhancement and approximate accumulation rate of the iodine liposomes. Animals were then separated into two groups. Animals in the "good prognosis" group had rapid and intense iodine enhancement in their mammography images, and were hypothesized to respond better to subsequent treatment with liposomal doxorubicin than those in the "bad prognosis" group, exhibiting slower, less pronounced iodine enhancement. Animals were then treated with liposomal doxorubicin and tumor growth was monitored. After treatment, tumor growth rates proved to be much slower in the good prognosis group, resulting in longer survival times than the bad prognosis group.

Karathanasis et al was able to monitor treatment with liposomal chemotherapeutics by using a multifunctional liposomal nanoparticle that encapsulated both iodine (contrast agent) and doxorubicin (chemotherapeutic) [79]. Mammographic imaging after administration of these nanoparticles enabled real time, non-invasive assessment of accumulation of drug within tumors. Having an a priori knowledge of the loading of each material allowed quantification of doxorubicin delivery to the area of interest. The encapsulation of iodine not only allowed one to track the accumulation of doxorubicin in the tumor, but also allowed one to track tumor response to the drug throughout treatment.

2.5 Nanoparticle Surface Modifications

The mononuclear phagocyte system (MPS) (formerly known as the reticuloendothelial system, or RES) is responsible for removal of macromolecules from the blood circulation [80]. The system is composed of blood monocytes, tissue macrophages, bone marrow progenitors, Kupffer cells of the liver, and macrophages in the spleen. Unprotected nanoparticles are cleared from the circulation by the MPS in as little as 2-3 hours. Though the circulation of these nanoparticles is much greater than that of the freely injected molecules which they encapsulate (as little as 5 minutes for drugs like doxorubicin), the short circulation times often do not allow enough time for sufficient accumulation of nanoparticles in passively targeted tumor tissue. Modification of the surface of the nanoparticle can help evade the MPS, resulting in longer circulation times and thus higher accumulation in target tissue.

The versatility of nanoparticles not only lies in the ability to package small molecules, but also in the many types of surface modifications that can be employed. Stealth liposomes containing the hydrophilic polymer PEG or polysaccarides on their surface can be used to protect nanoparticles from MPS clearance. These molecules are greatly hydrophillic and effectively create a layer of water surrounding the nanoparticle, reducing exposure to blood proteins and thus preventing opsonization of the nanoparticle. Opsonization marks macromolecules for phagocytosis by immune cells. The coating also reduces exposure of the nanoparticle to the immune cells themselves. Coatings can aid in steric stabilization of nanoparticles, as well as prevent interactions between nanoparticles such as those that could lead to agglomeration.

Surface modifications allow one to make hydrophilic, hydrophobic, or amphipathic nanoparticles. Other surface modifications allow attachment of ligands such as proteins, antibodies, peptides, nucleic acids, and other small molecules that turn nanoparticles into cell specific targeting vehicles [81-83].

One example of molecular targeting of nanoparticles is the use of surface bound folate on PEGylated stealth liposomes to target 9L glioma, which over-express folate receptors [84]. Though these nanoparticles proved promising in vitro, their use in vivo did not produce the anticipated increased efficacy over non-targeted stealth liposomes [85]. The presence of folate on the surface on the liposomes counteracted the stealth nature of the PEGylated liposomes, allowing opsonization and accelerated clearance from the blood stream. McNeeley et al proposed a solution using longer cleavable PEG chains to mask the folate molecules until accumulation in the tumor occurred [86]. PEG molecules with molecular weight of 5000 Daltons were bound to the liposome surface via a cleavable disulfide bond. The longer PEG chains masked the folate targeting molecules, which were attached to 2000 Dalton PEG molecules. The liposomes were able to evade the MPS and accumulate in the tumor via the EPR effect. Later, cysteine was delivered to cleave the disulfide bond and detach the PEG_{5000} coating. This exposed the folate molecules and allowed them to bind to the folate receptors of the target 9L gliomas cells, resulting in increased uptake and cell death compared to control non-targeted stealth liposomes.

2.6 Conclusion

Several types of nanoparticles could be used to deliver a small molecule visible dye to a tumor to stain it. However, in order to rapidly employ such a particle in clinic,

23

the nanoparticle used should be biocompatible and safe for use in humans. Carbon nanotubes show promise, but little is known about their long term biocompatibility. It is likely that dendrimers would not stably encapsulate sufficient amounts of dye to effectively stain the tumor. Metallic nanoparticles have similar problems to carbon nanotubes; though they are inert, many of the particles remain within the body indefinitely after treatment, making chronic complications probable, especially with multiple injections. Polymeric nanoparticles are likely safe, but none have been FDA approved for use in cancer therapy at this time. Liposomes have been FDA approved for many drug and contrast delivery applications, including chemotherapy and treatment of fungal infections. Thus, we opted to employ liposomal nanocarriers to encapsulate a visible dye for tumor border delineation in vivo. In the following sections, a method of staining tumors with a nano-encapsulated visible dye is presented.

24

CHAPTER 3

METHODS AND MATERIALS

3.1 Choosing a Dye and Perceived Luminance

Dyes were evaluated for perceived luminance, which estimates the darkness of a color. Dyes were dissolved in phosphate buffered saline (PBS) at the same concentration (m/v), dilute enough for all dyes to remain translucent when contained in a 1.5 mL microcentrifuge tube. An image was taken of all the dyes together to ensure consistent lighting conditions. RGB values were measured in 3 places for each dye using the color picker tool in Photoshop (Adobe, San Jose, CA) and averaged. Luminance was calculated via the following equation [87]:

$$(1)\ 0.299*R + 0.587*G + 0.114*B$$

3.2 Liposomal Nanocarrier Preparation

Liposomal nanocarriers were prepared using a mixture of 1,2–Dipalmitoyl-sn-glycero-3-phosphocholine (DPPC) (Genzyme, Cambridge, MA), cholesterol (Sigma-Aldrich, St Louis, MO), and N-(carbonyl-methoxypolyethyleneglycol-2000)-1,2-distearoyl-sn-glycero-3-phosphoethanolamine (MPEG-2000-DSPE) (Genzyme) in a 55:40:5 molar ratio dissolved in ethanol. Nano-EB particles were made by hydrating the lipid mixture using 75 mg/ml of Evans blue (Alfa Aesar, Ward Hill, MA) in PBS while blank liposomes were made by hydrating with PBS alone. The solution was stirred at 60°C for 120 minutes then dialyzed overnight against isosmolar PBS to remove ethanol. The liposomes were resized by placing the suspension in a Branson 1510 bath sonicator (Branson Ultrasonics, Danbury, CT) for 120 minutes at 60°C. Nano-EB particles were then run through a Sepharose CL-4B (GE Healthcare, Pittsburgh, PA) size exclusion

25

chromatography column to remove excess, unencapsulated dye. The filtrate was run through a 500kD MWCO MicroKros diafiltration cartridge (Spectrum Laboratories, Rancho Dominguez, CA) to remove volume gained in the column.

3.3 Liposomal Nanocarrier Analysis and Characterization

Liposomal nanocarriers were analyzed to obtain size distribution and lipid to dye ratio, as well as for stability in conditions similar to those encountered in vivo. Size distribution of the liposomal nanocarriers was determined using a Zetasizer Nano ZS90 dynamic light scattering (DLS) particle sizer (Malvern Instruments Ltd, Worcestershire, UK).

Lipid to dye ratio was calculated as amount of lipid divided by amount of dye (mg/mg). First, the amount of encapsulated dye in the liposome solution was determined by measurement of absorbance of EB. Liposomes were lysed in 0.8% Triton X100 to release their contents and absorbance was measured at 610 nm using a Synergy HT Plate Reader (BIO-TEK, Winooski, VT) and compared to a standard curve.

Final lipid concentration in the liposomal nanocarrier suspension was obtained by quantifying the fluorescence of a reporter molecule included in the original liposome mixture. β-DPH-HPC (Invitrogen, Carlsbad, CA) was included in the liposome mixture at a concentration of 0.01 mol%. After liposome preparation was complete, lipid and dye in a 100 µL sample were separated via Folch extraction [88]. Dried lipid extract was resuspended in ethanol and fluorescence was measured in a Synergy HT Plate Reader (BIO-TEK, Winooski, VT) (Excitation: 360 nm Emission 460 nm). A standard curve of known concentrations of β-DPH-HPC was used to calculate the amount of lipid present in the mixture.

Liposomal nanocarrier stability measurement was adapted from methods used for stability of doxorubicin containing liposomes [89]. Briefly, liposomal nanocarriers were placed in a 50% fetal bovine serum (FBS) (Gemini Bio-Products, West Sacramento, CA) in PBS solution to imitate blood serum. Nanocarriers were present at a concentration low enough to eliminate self quenching of the dye. The solution was placed in a 37°C water bath and samples were taken at 0, 24, and 48 hours. Leak of dye from the nanocarriers was assessed by measuring fluorescence of the samples at excitation 620 nm, emission 680 nm. Percent leak was calculated as follows:

(2) % leak = [(sample intensity)$_T$ – (sample intensity)$_{T=0}$] / [(sample intensity)$_{lysed}$ – (sample intensity)$_{T=0}$]

where T is the time point, T=0 is the initial time point (representing zero leak), and lysed indicates a sample lysed using 0.8% Triton X-100 (Sigma-Aldrich, St Louis, MO) (representing 100% leak).

3.4 Cell Culture

3RT1RT2A (rat glioma cell line, stably expresses green fluorescent protein, GFP) were generously donated by Helen L. Fillmore (Virginia Commonwealth University, Richmond, VA). Cells were cultured in Dulbecco's Modification of Eagle's Medium with 4.5 g/L glucose without L-glutamine and sodium pyruvate (Mediatech, Manassas, VA), supplemented with 10% FBS, 1% penicillin/streptomycin (Mediatech), 1% non-essential amino acids (Mediatech), 1% L-glutamine (HyClone Thermo Scientific, Logan, UT), and 1mg/ml G418 (Gemini Biosciences, West Sacramento, CA) as selective pressure for the GFP marker. Primary cortical rat astrocytes were obtained and cultured as described previously [90].

27

3.5 In Vitro Cell Viability

Primary astrocytes, representing normal brain tissue, and 3RT1RT2A cells, representing aggressive glioblastoma, were used to assess viability of cells treated with nano-EB in vivo. Astrocytes were plated at 10,000 cells per well, while 3RT1RT2A cells were plated at 25,000 cells/well, in tissue culture treated 24 well plates. Cells were treated for 24 hours with serum free media containing either nano-EB, unencapsulated EB in saline, blank liposomes, or sterile saline as a control. EB dose was 0.2 mg/ml in both nano-EB and unencapsulated EB solutions; the dose was chosen under the assumption that a maximum of 2% of the liposomes delivered to an animal would reach the tumor based on previous work in the lab with similar liposomal nanocarriers [85]. The lipid dose was equal in the two liposomal groups. After 24 hours, the treatments were removed and fresh appropriate standard serum containing cell culture medium was added. Cell viability counts were taken at 0, 24, 48, and 72 hours using the CCK-8 counting kit (Dojindo, Rockville, MD) as per the manufacturer's instructions. Cell counts were normalized to the untreated groups at each time point and reported as percent viable cells. Statistical significance was determined using a 2-way ANOVA with Tukey's post test using GraphPad Prism (Graphpad, La Jolla, CA). Data is presented as average ± standard deviation.

3.6 Ethical Use of Animals

All animal protocols were approved by the Georgia Institute of Technology Institutional Animal Care and Use Committee. Fisher 344 male rats 8-10 weeks of age were purchased from Harlan Laboratories. Animals were housed in a temperature

controlled environment with a 12 hour light/dark cycle, and were provided food and water for the entire duration of their housing.

3.7 In Vivo Toxicity Testing

Non-tumor bearing male Fisher 344 rats were injected via tail vein with sterile solutions of nano-EB, blank liposomes, or unencapsulated EB dye dissolved in saline. To ensure safety and sterility, all solutions were analyzed for correct pH and osmolarity, as well as tested for endotoxins (Lonza, Walkersville, MD), then filtered through a 0.2 µm sterile filter. Dye dose was 25 mg/kg in the two Evans blue formulations and lipid dose was kept equal in the two liposomal treatment groups. Mass and overall condition of the animals were monitored over a period of 4 weeks.

3.8 Tumor Implantation

Tumor implantation was adapted from Fillmore and colleagues [91]. Rats were anesthetized initially using 5% isofluorane and maintained at 2-3% during the entire procedure. Briefly, animals were placed in a stereotactic frame, an incision was made to expose the skull, and a burr hole was made at the coordinates of 2 mm anterior and 2 mm left lateral from lambda. 3RT1RT2A GFP expressing rat glioma cells were slowly injected 3 mm below the surface of the skull at this position over the course of 3 minutes (200,000 cells in 10 µL Liebovitz L-15 medium (Invitrogen Life Technologies/GIBCO, Carlsbad, CA)). Tumors were present in all animals that were injected in this way. Tumors implanted typically resulted in death by day 12-14; for this reason, animal experiments were constrained to 10 days.

29

3.9 Tumor Staining In Vivo

On day 8 of tumor growth, animals were injected via tail vein with sterile, non-pyrogenic solutions of 40 mg/kg EB, either as nano-EB or EB in sterile saline solution. Animals were euthanized 48 hours later and brains were removed and preserved in a 4% paraformaldehyde solution.

3.10 Visual and Histological Analysis of Tumor Staining

Brains of animals were removed and preserved in 4% paraformaldehyde in PBS. Brains were sliced coronally through the tumor and tumors were visually inspected to confirm presence of blue staining. Tissue was then cryoprotected by submersion in a 30% w/v solution of sucrose in PBS. Sections of 16 µm thickness were obtained using a Leica CM 300 cryostat (Leica, Bannockburn, IL). Sections were stained with anti-GFP monoclonal antibody conjugated with Alexa Fluor 488 (Invitrogen) to enhance green fluorescence and DAPI (Invitrogen) to indicate nuclei. Microscopic images of the entire tumor (5x magnification) were obtained and tiled together using a Axiovert 200M microscope (Zeiss, Thornwood, NY) with a ORCA-ER camera (Hamamatsu Photonics, Bridgewater, NJ) and Volocity acquisition software (PerkinElmer, Walthamm, MA).

Images were imported to ImageJ (NIH) where background subtraction was performed using the included rolling ball background subtraction algorithm. Images were converted to 8-bit and Manders Coefficients plugin was used to find Manders colocalization R and M1 (red:green, indicates how much red staining is also green) [92]. Additionally, the 8 bit images were used to trace the tumor border as well as the Evans blue staining border in the nano-EB treated samples. The measure function was used to obtain area and perimeter of the tracing. A ratio of red area to green area and red

30

perimeter to green perimeter were calculated. Data is presented as average ± standard deviation.

Higher magnification fluorescence images (10x magnification) of the tumor border were taken at 0, 90, 180, and 270 degrees around the border of the tumor to visually confirm that there was no healthy tissue staining.

CHAPTER 4

RESULTS

4.1 Liposomal Nanocarrier Fabrication and Characterization

For nanocarrier fabrication, a visible dye that would produce a high contrast to inherent brain tissue color was desired. Color wheel analysis showed that, other than black, blue and dark green offered the highest contrast to tissue encountered during surgery, including red (blood) and yellow/grey (healthy brain tissue). At identical concentrations, EB was visibly darker than any of the other dyes considered (Figure 1). This was confirmed by calculating perceived luminance of each dye, where a lower perceived luminance correlates with a darker color (values superimposed on Figure 1). EB had a perceived luminance value of 27, approximately 21% lower than the next darkest dye, Coomassie blue. Further, EB was more soluble than any of the other dyes, being 7 times more soluble than the next most soluble dye (EB 280g/L, Methylene blue 40 g/L). The liposomal nanocarrier core is aqueous so high solubility in water is desirable for maximum loading of dye.

Nano-EB particles were developed and characterized, assessing size, drug to lipid ratio, and stability. After processing was complete, the ratio of dye to lipid was 0.08 mg EB to 1 mg lipid. Average hydrodynamic diameter of nanocarriers was 173 nm with a polydispersity index of 0.1. Nano-EB particles were stable at body temperature (37°C), leaking only 13.3% (SD = 0.49%) of their contents over a 48 hour period.

Figure 1. Candidate dyes and perceived luminance. Dyes in solution at equal concentrations (m/v) and physiological pH. From left to right: Evans Blue (chosen for use in our experiments), Coomassie blue, methylene blue, bromophenol blue, lissamine green. Perceived luminance values are provided above each dye. Lower luminance correlates with darker appearance.

4.2 In Vitro and In Vivo Toxicity Assessment

To ensure nano-EB had no significant cytotoxic effects against healthy cells it was tested against both a glioma cell line and non-malignant primary astrocytes. Nano-EB treatment resulted in no significant changes in cell viability compared to blank stealth liposomes in either healthy primary astrocytes or the 3RT1RT2A glioma (Figure 2).

Non-tumor bearing animals were injected with either nano-EB, EB in saline, or blank liposomes and mass and general health of the animals were monitored for 4 weeks. All animals consistently gained weight after injection (Figure 3) and showed no visible signs of distress over the monitoring period. Animals injected with nano-EB remained slightly tinted blue for an average of 2 weeks post injection, while those injected with unencapsulated EB remained tinted blue for the entire span of the experiment.

33
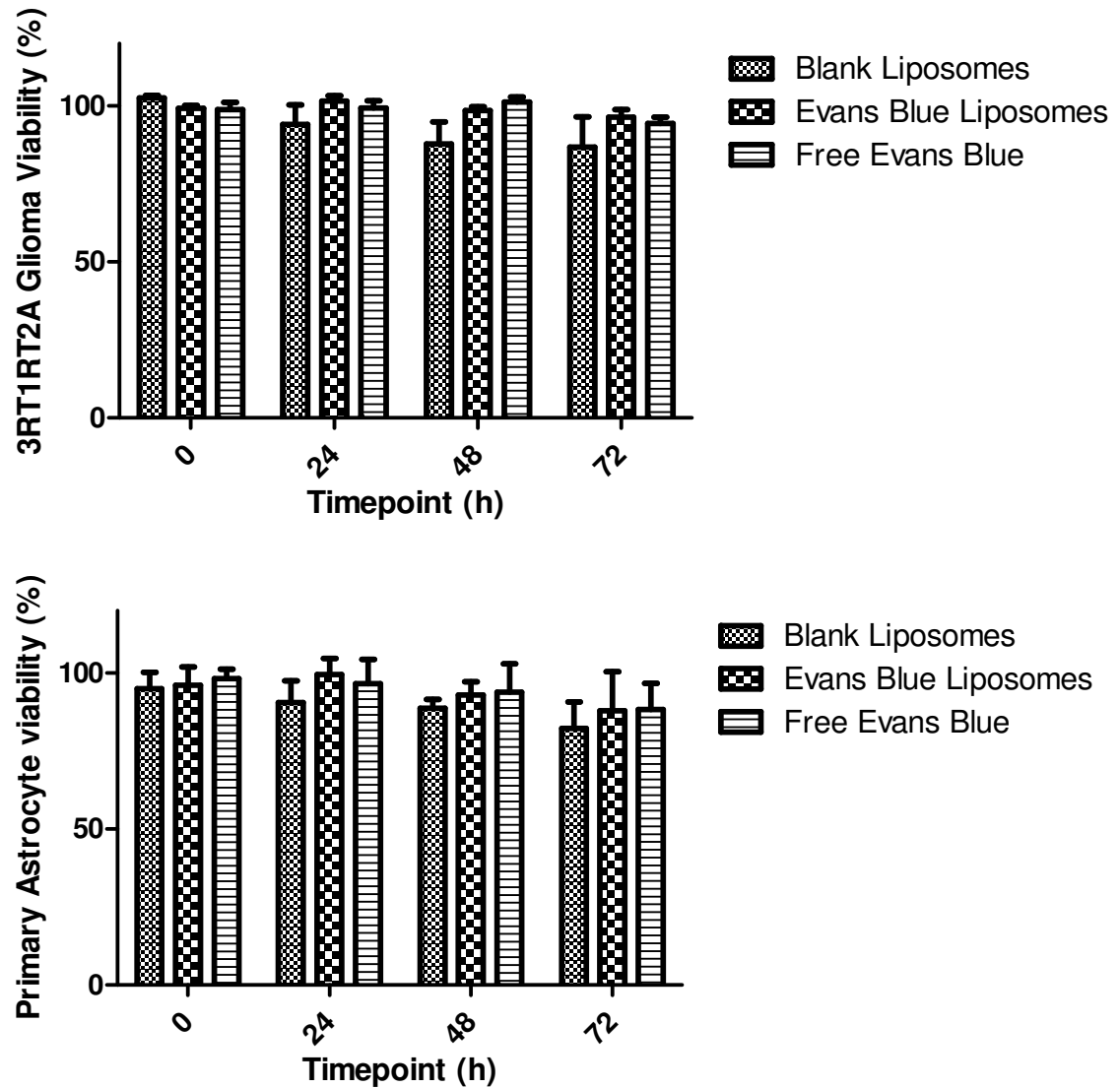
Figure 2. Cell viability after treatment. Cells were treated with either 0.2 mg/ml nano-EB or EB, or blank liposomes. Lipid dose of blank liposomes matched that of the nanoencapsulated Evans blue. All values normalized to PBS treated control.
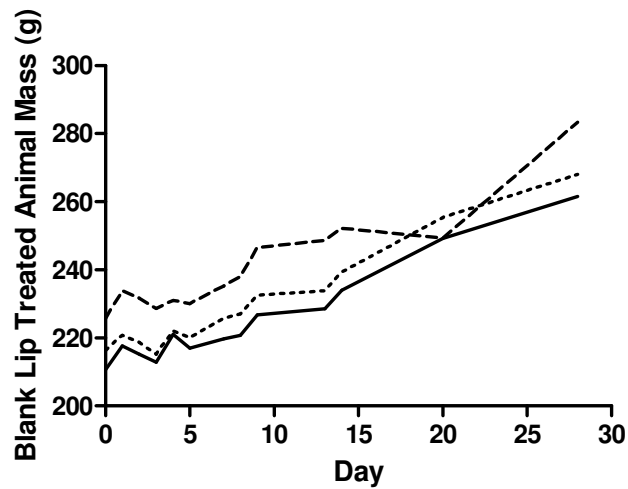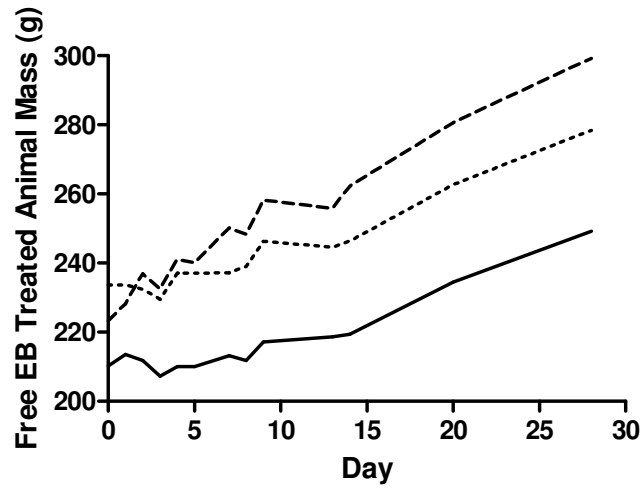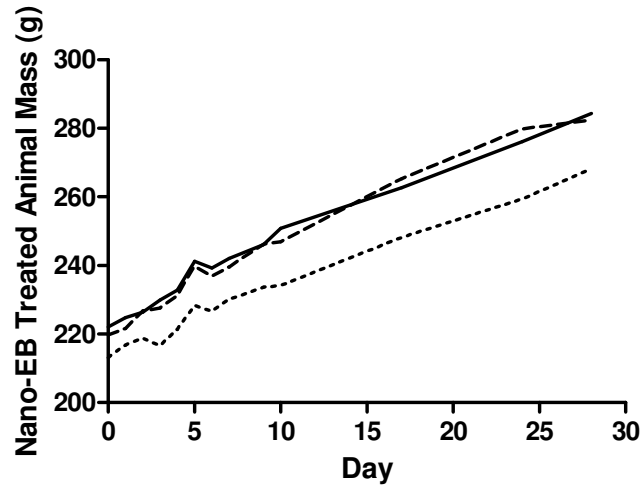
Figure 3. In vivo animal growth after treatment. Non-tumor bearing animals were injected with either nano-EB, unencapsulted EB, or blank liposomes. All animals steadily gained weight after injections.

4.3 Tumor Staining and Visualization In Vivo

Brains were sliced coronally through the center of the tumor to macroscopically show the extent of tumor staining evident to the naked eye (Figure 4). Brains of animals given unencapsulated EB showed diffuse staining in and around the tumor, with dye diffusing from the tumor into the healthy tissue. It should be noted that EB does not cross an intact blood brain barrier. Brains of animals given nano-EB only had staining in the region of the tumor.
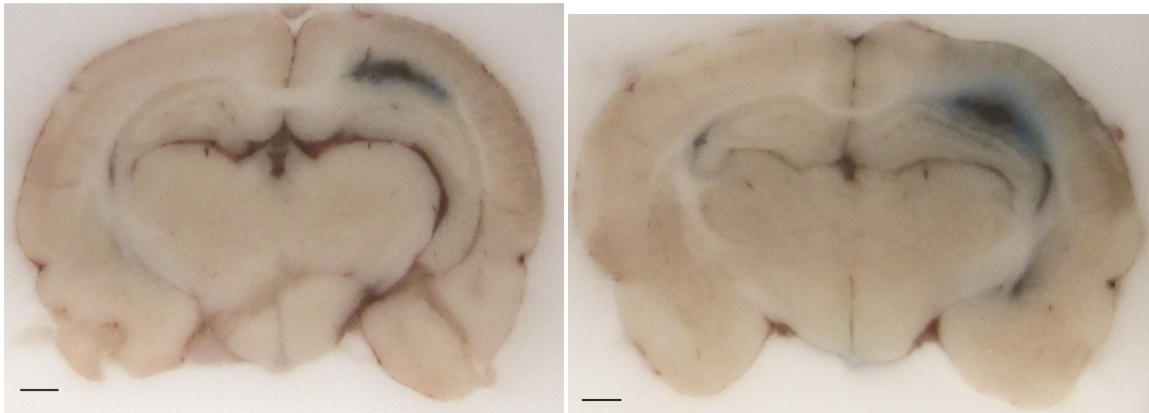
Figure 4. Coronal slice of brains of tumor bearing animals. Animals were treated with nano-EB (left) or EB (right). Scale bars = 1mm

Besides its contrasting blue color, EB also fluoresces red, making high magnification microscopic analysis possible. Fluorescence microscopy was performed to confirm that nano-EB did not stain healthy tissue (Figure 5). Manders coefficient analysis was performed on tiled whole tumor images, comparing green fluorescence from GFP expressing tumor cells with red fluorescence of the nano-EB (results in Table 1). Average overall Manders R was found to be 0.51 ± 0.08 (n=3 animals, 3 slices per animal). M1 (red:green) was found to be 0.97 ± 0.06, indicating that 97% of the red fluorescence colocalized with green fluorescence.

المنارة للاستشارات

www.manaraa.com
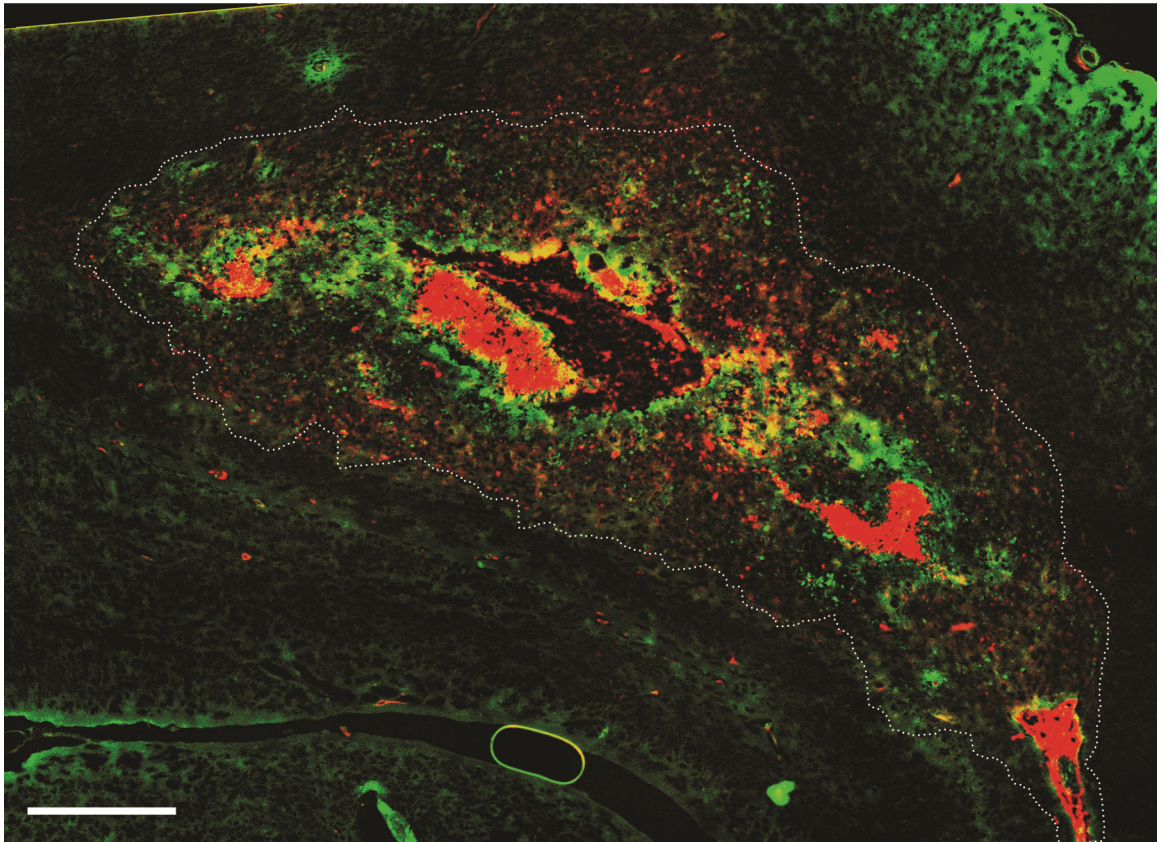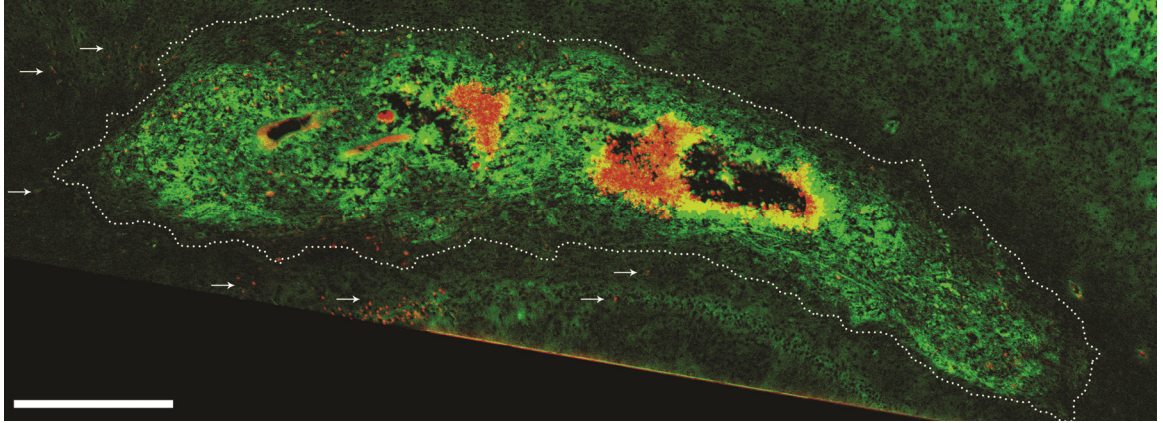
Figure 5. Microscopic analysis of staining. Whole tumor stitch, 5x magnification. (Top) Tumor of nano-EB treated animal. Green indicates tumor cells (GFP). Red indicates EB. Arrows indicate invasive clusters of cells marked by nano-EB. (Bottom) Tumor of Free EB treated animal. Scale bars = 500 µm

Further analysis compared the total area of the tumor to that of the nano-EB stained tissue to get an indication of how much of the total tumor was stained. Ratio of red area to green area averaged 0.89 ± 0.05. The ratio of perimeter of the same slices was 0.94 ± 0.04. Numbers close to but not greater than 1 indicate that the nanocarrier staining of tissue always stayed within the tumor tissue. Lack of healthy tissue staining was confirmed by visually inspecting high magnification (10x) images of the tumor border in nanocarrier treated animals (Figure 6).

Table 1. Border Quantification of Tumor Bearing Animals treated with Nano-EB.

Area Ratio[*]	Perimeter Ratio[**]	Manders R[#]	M1 (red:green)[##]
.89 ± .05	.94 ± .04	.51 ± .08	.97 ± .06

[*]Area ratio = area red (nano-EB) / area green (3RT1RT2A glioma cells, GFP).
[**]Perimeter ratio = perimeter red/perimeter green.
[#]Manders R indicates the amount of colocalization of red and green throughout the tissue.
[##]M1 indicates how much tissue stained red is also stained green.
N = 3 animals, 3 tissue sections per animal.
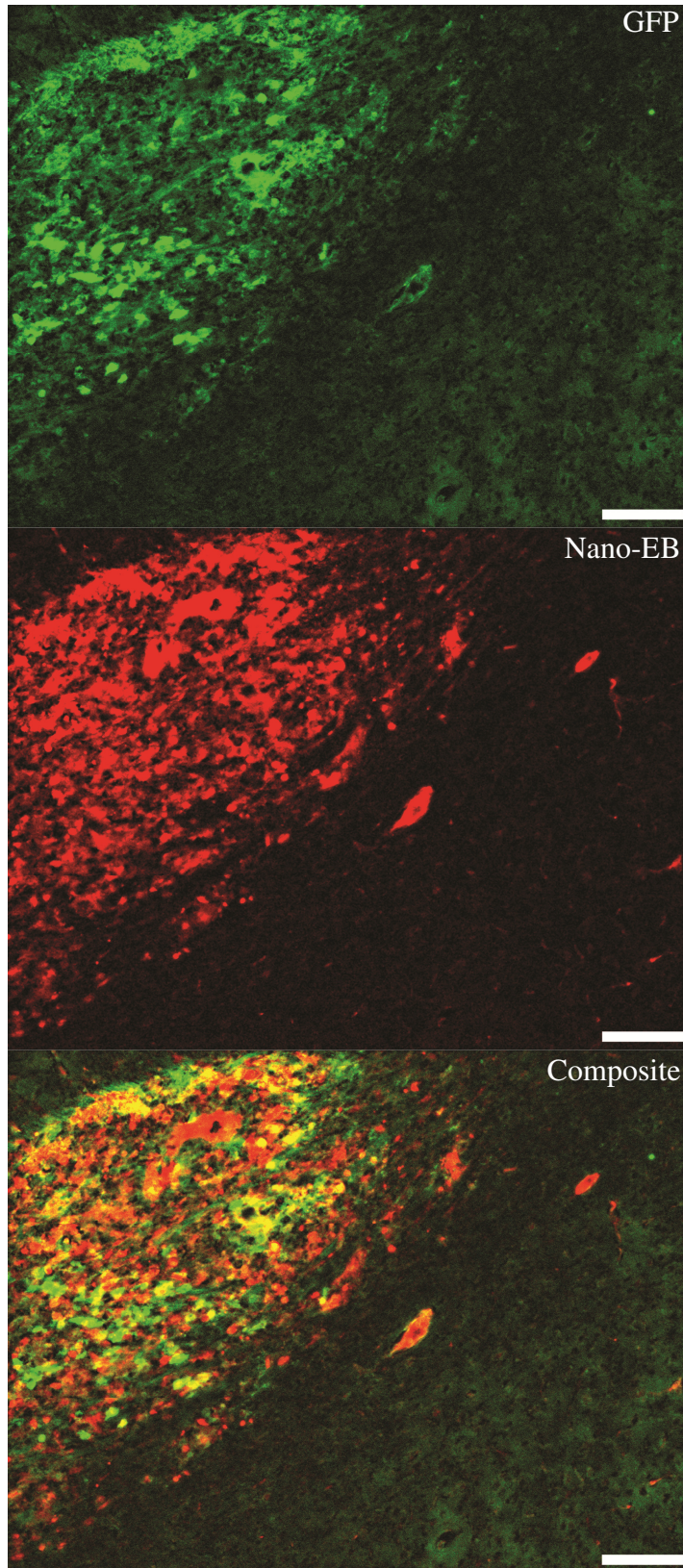
Figure 6. Tumor Border Images of nano-EB treated animals. (Top) Tumor (GFP) (Middle) Nano-EB (red fluorescence). (Bottom) Composite image. Scale bars = 100 µm

CHAPTER 5

DISCUSSION AND CONCLUSION

5.1 Discussion

Complete resection of tumor is essential to successful treatment of gliomas. Currently, once resection has begun, the surgeon has limited ability to distinguish the margin of the tumor, relying on subjective criteria such as tactile feedback and slight, often indistinguishable, color differences between healthy and tumor tissue. Thus, it would be beneficial to have an objective means to distinguish the tumor margin visually for the neurosurgeons in the OR. Other approaches include staining tumors using fluorescent molecules, but these require specific lighting conditions since the halogen lights typically used in surgical environments often emit radiation in the wavelengths that causes interference with fluorescence detection, as well as extra equipment and training [11-15]. In response, non-fluorescent dyes have been tested, though these compounds were only tested in non-invasive tumor models, which may not adequately represent their use clinically [16, 17].

Here, we demonstrate that freely circulating small molecule compounds, such as Evans blue dye, diffuse out of the tumor and in to healthy tissue complicating their ability to help demarcate the margins between tumor and healthy tissues. We proposed the use of a nano-scale encapsulation of a visible dye to provide the objective criteria that surgeons need to consistently and correctly distinguish tumor tissue from healthy tissue without the need of specialized equipment, lighting, or extra training on new equipment.

Intravenous injection of liposomal nanocarriers containing Evans blue dye clearly marked the tumor and its margins, as well as small nodules of invasive cells that had

40

invaded beyond the bulk tumor border. A Manders coefficient of 0.6 or higher is generally accepted as indicating true colocalization in fluorescence microscopy [93]. In our experiments, we obtained Manders coefficients that appear low at 0.51 ± 0.08, but this was to be expected. Little endocytosis by cancer cells of the nano-EB occurs at the time scale used (48h). Therefore, most would be present extracellularly and thus not overlap with cytoplasmic GFP.

An important measure obtained from overlap coefficient analysis is the M1 (red:green) of 0.97, indicating that nearly all area that was stained red was also stained green. This indicates that nanocarriers stained only tumor tissue. The area and perimeter ratio analysis further confirmed that the nanocarriers only stained tumor tissue. Higher magnification microscopic examination of the border also confirmed that only tumor tissue was stained, with nanocarriers slightly and consistently underestimating the true margin on the order of tens to hundreds of micrometers. This is sufficient considering surgeons often remove tissue in sections with thicknesses on the order of millimeters, several orders of magnitude greater than the underestimation [94]. It is important to note that healthy tissue was not stained, preventing false positives and removal of healthy tissue by the surgeon.

The amount of leak of dye from the liposomes over the 48 hour period after injection was consistent with previously reported clinically used liposomal nanocarrier formulations [72, 95, 96]. It should be noted that even with this slight leak the nano-EB did not stain healthy tissue. Evans blue is a strongly polar molecule; leaked dye quickly binds to blood serum proteins, limiting its diffusion [97].

41

Evans blue dye was initially FDA approved for use in blood volume measurement. It was later found to be toxic in repeated use or large doses [98, 99]. However, the negative side effects are usually reduced and pharmacokinetics of molecules are drastically changed when they are encapsulated in liposomal nanocarriers [21-23, 85]. The encapsulation of molecules creates a barrier and reduces their ability to interact with non-target tissues. For example, the nanoencapsulation of doxorubicin in liposomes known as Doxil®; cardiotoxicity is greatly reduced in Doxil® when compared to free drug [22, 23].

In vitro, nano-EB did not have a negative effect on the viability of either the tumor cell line (3RT1RT2A) or their healthy counterpart, primary astrocytes. Intravenous injections of either nano-EB or EB had no negative effect on the growth of animals treated, nor did it cause any visible signs of distress in the animals. This was to be expected since the doses used were much lower than those seen as toxic in published studies [98, 99]. Emphasis should be placed on further testing to determine the safety of such a nanocarrier for clinical use.

Our data demonstrates that tumor margins may be reliably and accurately demarcated by eliminating the staining of healthy tissue seen when small molecule dyes are used in an invasive tumor model. It also demonstrates that nanocarriers carrying visible dyes localize to tumor margins facilitating both the accurate resection of the tumor and accurate sparing of healthy tissue.

5.2 Conclusion

Liposomal nanocarriers containing visible dye Evans blue (nano-EB) successfully stain invasive tumors in vivo, creating clear visible distinction between tumor and healthy

tissue. A nanocarrier is not only preferred but also necessary; injection of unencapsulated dye results in staining of healthy tissue in an invasive tumor model. Invasive models are more clinically relevant than non-invasive models such as 9L. Use of such a nanocarrier would allow surgeons to intraoperatively distinguish tumor tissue from healthy, likely increasing extent of resection, and thus result in a better prognosis for the patient while preserving function and quality of life.

CHAPTER 6

FUTURE DIRECTIONS

6.1 Dose and Time Point Optimization

The dosing in this study was not optimized for maximum staining while minimizing side effects, such as coloration of the animal. Basically, it was a brute force method used in order to get the desired result. The maximum volume injection was used with the maximum concentration of liposome encapsulated EB possible. In theory, the same results could be reached using much lower doses. PEG coated liposomes typically circulate for long periods of time, with half lives on the order or 1-3 days. Longer circulation times allow for higher accumulation in tumor tissue based on probability. The more times a particular liposome passes by the fenestrated vasculature in the tumor, the more likely it is to extravasate into the tumor interstitium. Therefore, if dose is reduced and time before surgical intervention is increased, similar results could be seen. Lower dose would decrease the blue tinting of the patient, as well as reduce likelihood of toxic side effects.

This approach, however, is limited by the leakiness of the liposomes themselves. If too much time is allowed, encapsulated dye would leak out in large enough concentrations that dye would diffuse into healthy tissue. The result would be healthy tissue staining and false positive marking, much like what is seen when unencapsulated Evans blue dye is injected.

During this study, the timepoint of 48 hours was chosen based on literature demonstrating the long circulating characteristics of similar formulations of liposomes {. However, these were either drug delivery or contrast enhanced non-invasive imaging

44

studies, so they do not necessarily apply here when visible contrast is the metric. Research should be done to assess the optimal time for sufficient accumulation to ensure visible contrast.

6.2 Nano-EB Staining in Other Tumor Models

Above, we have shown that a nanoencapsulated visible dye will accurately and reliably stain an invasive tumor without staining healthy tissue. However, this was only done in one animal model of rat glioma, RT2. Though RT2 is a well known clinically relevant form of invasive glioma, it would be necessary to show effectiveness in other tumor models. This should include other models in the rat, including the non-invasive 9L model used by fellow researchers attempting to develop visible dyes to stain brain tumors. Models of medulloblastoma and other malignant tumors of the CNS should also be considered. Future research should also include tumor models in higher organisms.

The presented method could be used in other tissues as well to mark tumors. Kaposi's sarcoma is a highly malignant skin cancer that is currently treated with liposomal doxorubicin. It is likely that nano-EB would effectively stain these lesions for resection. It is likely the method would not work in tissues such as the liver and spleen. One of the many jobs of the liver is to filter macromolecules out of the blood. The spleen is part of the MPS, a system responsible for removing macromolecules throughout the body. Therefore, excess nano-EB liposomes accumulate in these tissues. As a result, the healthy regions of the tissues themselves would be stained blue so there would not be sufficient contrast between tumor tissue and background accumulation in these tissues.

45

6.3 Reducing Production Time and Waste

The manufacturing process by which the nano-EB particles were made is very time consuming, messy, labor intensive, and produces a lot of waste. Evans blue dye was dissolved at 75 mg/ml in the initial solution to ensure the maximum possible loading of the aqueous core of the liposomes. The unencapsulated dye then had to be removed to avoid healthy tissue staining in vivo. Several purification techniques were attempted, including dialysis, diafiltration, high speed centrifugation, and spin columns, but only size exclusion chromatography columns proved sufficient to nearly completely remove unencapsulated dye. Even though the technique worked, it required multiple passes of the crude liposome mixture through the separation column to ensure enough dye was removed so that the nanocarriers could be used in vivo. Also, column chromatography is not conducive to scale up. Generally diafiltration is the optimal scalable process for purification of liposomes for the large scale manufacturing processes necessary for a product to be used in clinic. Though it would require synthesis of a new dye molecule, excess wasted dye could be reduced if an active loading scheme were used opposed to the passive scheme currently employed.

Loading of doxorubicin into liposomes is an example of active loading. This method was first published by Bolotin et al in 1994 [100]. First, liposomes are manufactured so that they contain acidic (pH~5 - 5.5) ammonium sulfate in their aqueous core. Then, doxorubicin is placed into the liposome suspension and heat is applied to cause the lipid bilayer to become fluid-like. Doxorubicin is initially amphipathic, allowing it to freely pass through the lipid bilayer into the aqueous core of the liposomes (Figure 7). When the molecule enters the slightly acidic core of the liposome, the

neutrally charged $-NH_2$ gains a hydrogen atom and becomes $-NH_3^+$. The newly formed positive charge ionically associates with sulfate (SO_4^-) present in the liposome core to form an insoluble precipitate. Thus, governed by the law of mass action, the reaction equilibrium is constantly driven to create more precipitate until either doxorubicin or sulfate ions are exhausted. A similar scheme could be employed using a dye similar to Evans blue, but with the properties of doxorubicin (an amphipathic molecule at neurtral pH that would gain a positive charge when exposed to lower pH).

Adapted from Bolotin et. al., J Liposome Res. 4(1), 1994
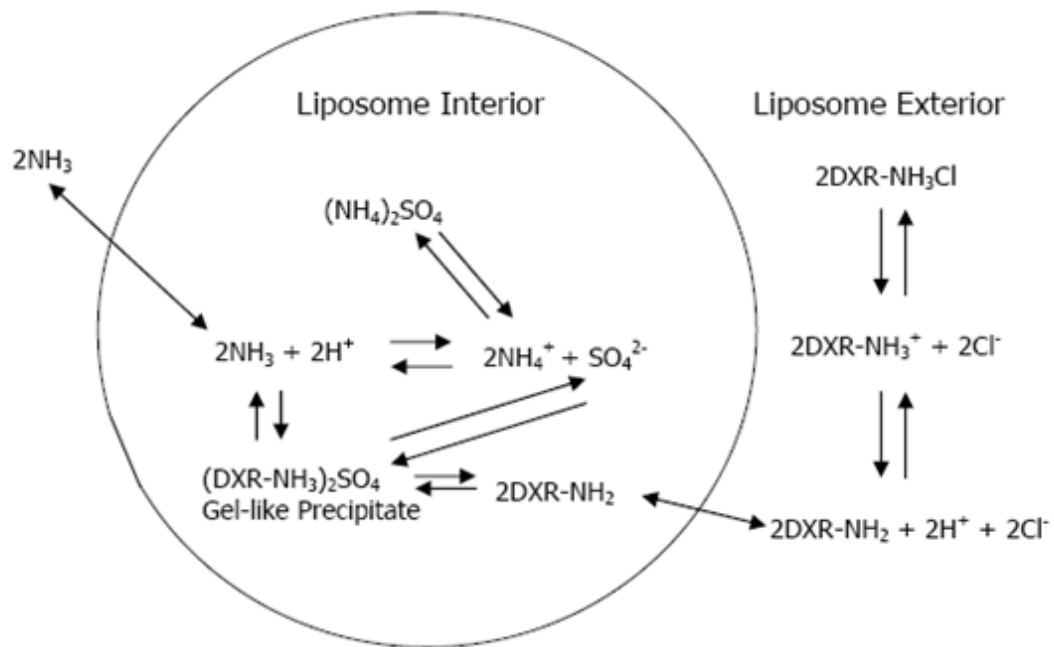
Figure 7. Ammonium sulfate gradient loading scheme for doxorubicin.

6.4 Developing a Dual Mode Nanocarrier

It would be beneficial if the nanocarrier could not only provide intraoperative delineation, but could also be used for non-invasive contrast enhancement of tumor for preoperative surgical planning. MRI is often used to provide a topographic map of the

brain and location of the tumor, which surgeons use to plan out their resection procedure. Thus, a nanocarrier that could provide MRI enhancement is desireable. Currently, it is common to use unencapsulated gadolinium (Gd) chelates to provide contrast for MRI for many applications, including tumor contrast enhancement. Development of such a nanocarrier would be straight forward.

Phospholipids that are conjugated to Gd chelates are available for purchase. Ghaghada et al. used such phospholipids to demonstrate effectiveness incorporating these phospholipid Gd chelates into liposomes for in vivo MRI imaging [101]. Manufacturing would be simple, only adding a few steps to the current manufacturing process. Essentially, one would manufacture the liposomes as presented in the methods section, then the Gd chelates can be post-inserted, similarly to the methods used by Saul et al to post insert folate conjugated phospholipids into liposomes [84].

A dual mode nanocarrier capable of MRI contrast as well as intraoperative tumor border delineation would allow for both to be performed after a single injection. Pharmacokinetics should be similar to nano-EB since the MW of the PEG chains is much larger than that of the Gd chelate. The chelate would be shielded from the MPS much like the surface of the liposome itself so opsonization and clearance will be slowed.

48

REFERENCES

1. C.B.T.R.o.t.U. States, E., *Primary Brain Tumors in the United States: Statistical Report 2000-2004*: Ogden, IL.

2. A.C. Society, E., *Cancer Facts & Figures*: Atlanta.

3. Guthrie, B.L. and E.R. Laws, Jr., *Supratentorial low-grade gliomas.* Neurosurg Clin N Am, 1990. **1**(1): p. 37-48.

4. Black, P., *Management of malignant glioma: role of surgery in relation to multimodality therapy.* J Neurovirol, 1998. **4**(2): p. 227-36.

5. Keles, G.E., B. Anderson, and M.S. Berger, *The effect of extent of resection on time to tumor progression and survival in patients with glioblastoma multiforme of the cerebral hemisphere.* Surg Neurol, 1999. **52**(4): p. 371-9.

6. Yasargil, M.G., P.A. Kadri, and D.C. Yasargil, *Microsurgery for malignant gliomas.* J Neurooncol, 2004. **69**(1-3): p. 67-81.

7. Clarke, J., N. Butowski, and S. Chang, *Recent advances in therapy for glioblastoma.* Arch Neurol, 2010. **67**(3): p. 279-83.

8. Sanai, N. and M.S. Berger, *Glioma extent of resection and its impact on patient outcome.* Neurosurgery, 2008. **62**(4): p. 753-64; discussion 264-6.

9. Choucair, A.K., et al., *Development of multiple lesions during radiation therapy and chemotherapy in patients with gliomas.* J Neurosurg, 1986. **65**(5): p. 654-8.

10. Mornex, F., H. Nayel, and L. Taillandier, *Radiation therapy for malignant astrocytomas in adults.* Radiother Oncol, 1993. **27**(3): p. 181-92.

11. Britz, G.W., et al., *Intracarotid RMP-7 enhanced indocyanine green staining of tumors in a rat glioma model.* J Neurooncol, 2002. **56**(3): p. 227-32.

12. Kircher, M.F., et al., *A multimodal nanoparticle for preoperative magnetic resonance imaging and intraoperative optical brain tumor delineation.* Cancer Res, 2003. **63**(23): p. 8122-5.

13. Pham, W., Z. Medarova, and A. Moore, *Synthesis and application of a water-soluble near-infrared dye for cancer detection using optical imaging.* Bioconjug Chem, 2005. **16**(3): p. 735-40.

14. Veiseh, M., et al., *Tumor paint: a chlorotoxin:Cy5.5 bioconjugate for intraoperative visualization of cancer foci.* Cancer Res, 2007. **67**(14): p. 6882-8.

15. Nguyen, Q.T., et al., *Surgery with molecular fluorescence imaging using activatable cell-penetrating peptides decreases residual cancer and improves survival.* Proc Natl Acad Sci U S A, 2010. **107**(9): p. 4317-22.

16. Ozawa, T., et al., *Bromophenol blue staining of tumors in a rat glioma model.* Neurosurgery, 2005. **57**(5): p. 1041-7; discussion 1041-7.

17. Orringer, D.A., et al., *The brain tumor window model: a combined cranial window and implanted glioma model for evaluating intraoperative contrast agents.* Neurosurgery, 2010. **66**(4): p. 736-43.

18. Stojiljkovic, M., et al., *Characterization of 9L glioma model of the Wistar rat.* J Neurooncol, 2003. **63**(1): p. 1-7.

19. Karathanasis, E., et al., *Tumor vascular permeability to a nanoprobe correlates to tumor-specific expression levels of angiogenic markers.* PLoS One, 2009. **4**(6): p. e5843.

20. Popovic, Z., et al., *A nanoparticle size series for in vivo fluorescence imaging.* Angew Chem Int Ed Engl, 2010. **49**(46): p. 8649-52.

21. Siegal, T., A. Horowitz, and A. Gabizon, *Doxorubicin encapsulated in sterically stabilized liposomes for the treatment of a brain tumor model: biodistribution and therapeutic efficacy.* J Neurosurg, 1995. **83**(6): p. 1029-37.

22. Safra, T., et al., *Pegylated liposomal doxorubicin (doxil): reduced clinical cardiotoxicity in patients reaching or exceeding cumulative doses of 500 mg/m2.* Ann Oncol, 2000. **11**(8): p. 1029-33.

23. O'Brien, M.E., et al., *Reduced cardiotoxicity and comparable efficacy in a phase III trial of pegylated liposomal doxorubicin HCl (CAELYX/Doxil) versus conventional doxorubicin for first-line treatment of metastatic breast cancer.* Ann Oncol, 2004. **15**(3): p. 440-9.

24. Louis, D.N., *Molecular pathology of malignant gliomas.* Annu Rev Pathol, 2006. **1**: p. 97-117.

25. Wen, P.Y. and S. Kesari, *Malignant gliomas in adults.* N Engl J Med, 2008. **359**(5): p. 492-507.

26. C.B.T.R.o.t.U. States, E., *CBTRUS Statistical Report: Primary Brain and Central Nervous System Tumors Diagnosed in the United States in 2004-2007.* 2011: Hinsdale, IL.

27. Kleihues, P., P.C. Burger, and B.W. Scheithauer, *The new WHO classification of brain tumours.* Brain Pathol, 1993. **3**(3): p. 255-68.

28. Louis, D.N., et al., *The 2007 WHO classification of tumours of the central nervous system.* Acta Neuropathol, 2007. **114**(2): p. 97-109.

29. Scherer, H.J., *Structural Development in Gliomas.* American Journal of Cancer, 1938. **34**(3): p. 333-351.

30. Gladson, C.L., R.A. Prayson, and W.M. Liu, *The pathobiology of glioma tumors.* Annu Rev Pathol, 2010. **5**: p. 33-50.

31. Kleihues, P., et al., *The WHO classification of tumors of the nervous system.* J Neuropathol Exp Neurol, 2002. **61**(3): p. 215-25; discussion 226-9.

32. Crawford, J.R., T.J. MacDonald, and R.J. Packer, *Medulloblastoma in childhood: new biological advances.* Lancet Neurol, 2007. **6**(12): p. 1073-85.

33. Chen, W., *Clinical applications of PET in brain tumors.* J Nucl Med, 2007. **48**(9): p. 1468-81.

34. Young, G.S., *Advanced MRI of adult brain tumors.* Neurol Clin, 2007. **25**(4): p. 947-73, viii.

35. Walker, M.D., et al., *Evaluation of BCNU and/or radiotherapy in the treatment of anaplastic gliomas. A cooperative clinical trial.* J Neurosurg, 1978. **49**(3): p. 333-43.

36. Stupp, R., et al., *Radiotherapy plus concomitant and adjuvant temozolomide for glioblastoma.* N Engl J Med, 2005. **352**(10): p. 987-96.

37. Keime-Guibert, F., et al., *Radiotherapy for glioblastoma in the elderly.* N Engl J Med, 2007. **356**(15): p. 1527-35.

38. Hochberg, F.H. and A. Pruitt, *Assumptions in the radiotherapy of glioblastoma.* Neurology, 1980. **30**(9): p. 907-11.

39. Westphal, M., et al., *A phase 3 trial of local chemotherapy with biodegradable carmustine (BCNU) wafers (Gliadel wafers) in patients with primary malignant glioma.* Neuro Oncol, 2003. **5**(2): p. 79-88.

40. Bostick, P.J. and A.E. Giuliano, *Vital dyes in sentinel node localization.* Semin Nucl Med, 2000. **30**(1): p. 18-24.

41. Morton, D.L., et al., *Technical details of intraoperative lymphatic mapping for early stage melanoma.* Arch Surg, 1992. **127**(4): p. 392-9.

42. Morton, D.L., et al., *Intraoperative lymphatic mapping and selective cervical lymphadenectomy for early-stage melanomas of the head and neck.* J Clin Oncol, 1993. **11**(9): p. 1751-6.

43.   Giuliano, A.E., et al., *Lymphatic mapping and sentinel lymphadenectomy for breast cancer.* Ann Surg, 1994. **220**(3): p. 391-8; discussion 398-401.

44.   Bilchik, A.J., et al., *Universal application of intraoperative lymphatic mapping and sentinel lymphadenectomy in solid neoplasms.* Cancer J Sci Am, 1998. **4**(6): p. 351-8.

45.   Tanaka, E., et al., *Image-guided oncologic surgery using invisible light: completed pre-clinical development for sentinel lymph node mapping.* Ann Surg Oncol, 2006. **13**(12): p. 1671-81.

46.   Maeda, H., et al., *Tumor vascular permeability and the EPR effect in macromolecular therapeutics: a review.* Journal of Controlled Release, 2000. **65**(1-2): p. 271-284.

47.   Maeda, H., *The enhanced permeability and retention (EPR) effect in tumor vasculature: the key role of tumor-selective macromolecular drug targeting.* Adv Enzyme Regul, 2001. **41**: p. 189-207.

48.   Moore, G.E., *Fluorescein as an Agent in the Differentiation of Normal and Malignant Tissues.* science, 1947. **106**(2745): p. 130-1.

49.   Cheng, M.K., et al., *Photoradiation therapy: current status and applications in the treatment of brain tumors.* Surg Neurol, 1986. **25**(5): p. 423-35.

50.   Perria, C., et al., *Photodynamic therapy of malignant brain tumors: clinical results of, difficulties with, questions about, and future prospects for the neurosurgical applications.* Neurosurgery, 1988. **23**(5): p. 557-63.

51.   Hansen, D.A., et al., *Indocyanine green (ICG) staining and demarcation of tumor margins in a rat glioma model.* Surg Neurol, 1993. **40**(6): p. 451-6.

52.   Qian, X., et al., *In vivo tumor targeting and spectroscopic detection with surface-enhanced Raman nanoparticle tags.* Nat Biotechnol, 2008. **26**(1): p. 83-90.

53.   Hobbs, S.K., et al., *Regulation of transport pathways in tumor vessels: role of tumor type and microenvironment.* Proc Natl Acad Sci U S A, 1998. **95**(8): p. 4607-12.

54.   Jang, S.H., et al., *Drug delivery and transport to solid tumors.* Pharm Res, 2003. **20**(9): p. 1337-50.

55.   Jain, R.K. and T. Stylianopoulos, *Delivering nanomedicine to solid tumors.* Nat Rev Clin Oncol, 2010. **7**(11): p. 653-64.

56.   Cheng, Y., et al., *Pharmaceutical applications of dendrimers: promising nanocarriers for drug delivery.* Front Biosci, 2008. **13**: p. 1447-71.

57. Baker, J.R., Jr., *Dendrimer-based nanoparticles for cancer therapy.* Hematology Am Soc Hematol Educ Program, 2009: p. 708-19.

58. Gupta, U., et al., *Dendrimers: novel polymeric nanoarchitectures for solubility enhancement.* Biomacromolecules, 2006. **7**(3): p. 649-58.

59. Kojima, C., et al., *Synthesis of polyamidoamine dendrimers having poly(ethylene glycol) grafts and their ability to encapsulate anticancer drugs.* Bioconjug Chem, 2000. **11**(6): p. 910-7.

60. Majoros, I., et al., *PAMAM dendrimer-based multifunctional conjugate for cancer therapy: synthesis, characterization, and functionality.* Biomacromolecules, 2006. **7**(2): p. 572-579.

61. Kukowska-Latallo, J., et al., *Nanoparticle targeting of anticancer drug improves therapeutic response in animal model of human epithelial cancer.* Cancer research, 2005. **65**(12): p. 5317.

62. Olson, E.S., et al., *Activatable cell penetrating peptides linked to nanoparticles as dual probes for in vivo fluorescence and MR imaging of proteases.* Proc Natl Acad Sci U S A, 2010. **107**(9): p. 4311-6.

63. Konda, S.D., et al., *Specific targeting of folate-dendrimer MRI contrast agents to the high affinity folate receptor expressed in ovarian tumor xenografts.* MAGMA, 2001. **12**(2-3): p. 104-13.

64. Ali-Boucetta, H., et al., *Multiwalled carbon nanotube-doxorubicin supramolecular complexes for cancer therapeutics.* Chem Commun (Camb), 2008(4): p. 459-61.

65. Liu, Z., et al., *Supramolecular chemistry on water-soluble carbon nanotubes for drug loading and delivery.* Acs Nano, 2007. **1**(1): p. 50-56.

66. Liu, Z., et al., *In vivo biodistribution and highly efficient tumour targeting of carbon nanotubes in mice.* Nature nanotechnology, 2006. **2**(1): p. 47-52.

67. Kam, N., et al., *Carbon nanotubes as multifunctional biological transporters and near-infrared agents for selective cancer cell destruction.* Proceedings of the National Academy of Sciences of the United States of America, 2005. **102**(33): p. 11600.

68. Zhang, Z., et al., *Delivery of telomerase reverse transcriptase small interfering RNA in complex with positively charged single-walled carbon nanotubes suppresses tumor growth.* Clinical Cancer Research, 2006. **12**(16): p. 4933.

69. Paasonen, L., et al., *Gold nanoparticles enable selective light-induced contents release from liposomes.* Journal of Controlled Release, 2007. **122**(1): p. 86-93.

70.   Wu, G., et al., *Remotely triggered liposome release by near-infrared light absorption via hollow gold nanoshells.* J. Am. Chem. Soc, 2008. **130**(26): p. 8175-8177.

71.   Huang, X., et al., *Cancer cell imaging and photothermal therapy in the near-infrared region by using gold nanorods.* J Am Chem Soc, 2006. **128**(6): p. 2115-20.

72.   Agarwal, A., et al., *Remote triggered release of doxorubicin in tumors by synergistic application of thermosensitive liposomes and gold nanorods.* ACS Nano, 2011. **5**(6): p. 4919-26.

73.   Sajja, H.K., et al., *Development of multifunctional nanoparticles for targeted drug delivery and noninvasive imaging of therapeutic effect.* Curr Drug Discov Technol, 2009. **6**(1): p. 43-51.

74.   Slotkin, J., et al., *Cellular magnetic resonance imaging: nanometer and micrometer size particles for noninvasive cell localization.* Neurotherapeutics, 2007. **4**(3): p. 428-433.

75.   Parveen, S. and S.K. Sahoo, *Polymeric nanoparticles for cancer therapy.* J Drug Target, 2008. **16**(2): p. 108-23.

76.   Gu, F., et al., *Precise engineering of targeted nanoparticles by using self-assembled biointegrated block copolymers.* Proc Natl Acad Sci U S A, 2008. **105**(7): p. 2586-91.

77.   Zhang, L., et al., *Nanoparticles in medicine: therapeutic applications and developments.* Clin Pharmacol Ther, 2008. **83**(5): p. 761-9.

78.   Bangham, A.D., *Liposomes: the Babraham connection.* Chem Phys Lipids, 1993. **64**(1-3): p. 275-85.

79.   Karathanasis, E., et al., *Multifunctional nanocarriers for mammographic quantification of tumor dosing and prognosis of breast cancer therapy.* Biomaterials, 2008. **29**(36): p. 4815-22.

80.   Hume, D.A., *The mononuclear phagocyte system.* Curr Opin Immunol, 2006. **18**(1): p. 49-53.

81.   Alivisatos, P., *The use of nanocrystals in biological detection.* Nature Biotechnology, 2003. **22**(1): p. 47-52.

82.   Sinha, R., et al., *Nanotechnology in cancer therapeutics: bioconjugated nanoparticles for drug delivery.* Molecular cancer therapeutics, 2006. **5**(8): p. 1909.

83.   Yezhelyev, M., et al., *Emerging use of nanoparticles in diagnosis and treatment of breast cancer.* The lancet oncology, 2006. **7**(8): p. 657-667.

84.   Saul, J.M., et al., *Controlled targeting of liposomal doxorubicin via the folate receptor in vitro.* J Control Release, 2003. **92**(1-2): p. 49-67.

85.   McNeeley, K., A. Annapragada, and R. Bellamkonda, *Decreased circulation time offsets increased efficacy of PEGylated nanocarriers targeting folate receptors of glioma.* Nanotechnology, 2007. **18**: p. 385101 (11pp).

86.   McNeeley, K.M., et al., *Masking and triggered unmasking of targeting ligands on nanocarriers to improve drug delivery to brain tumors.* Biomaterials, 2009. **30**(23-24): p. 3986-95.

87.   International Telecommunications Union, R., *Rec. BT. 601-4, Encoding parameters of digital television for studios.* 1994.

88.   Folch, J., M. Lees, and G.H.S. Stanley, *A Simple Method for the Isolation and Purification of Total Lipides from Animal Tissues.* Journal of Biological Chemistry, 1957. **226**(1): p. 497-509.

89.   Gaber, M.H., et al., *Thermosensitive liposomes: extravasation and release of contents in tumor microvascular networks.* Int J Radiat Oncol Biol Phys, 1996. **36**(5): p. 1177-87.

90.   Karumbaiah, L., et al., *Targeted downregulation of N-acetylgalactosamine 4-sulfate 6-O-sulfotransferase significantly mitigates chondroitin sulfate proteoglycan-mediated inhibition.* Glia, 2011. **59**(6): p. 981-96.

91.   Fillmore, H.L., et al., *An in vivo rat model for visualizing glioma tumor cell invasion using stable persistent expression of the green fluorescent protein.* Cancer Lett, 1999. **141**(1-2): p. 9-19.

92.   Manders, E., F. Verbeek, and I. Aten, *Measurement of co-localization of objects in dual-colour confocal images.* J Microsc, 1993. **169**: p. 375-375.

93.   Zinchuk, V. and O. Zinchuk, *Quantitative colocalization analysis of confocal fluorescence microscopy images.* Curr Protoc Cell Biol, 2008. **Chapter 4**: p. Unit 4.19.

94.   Raore, B., et al., *Metastasis Infiltration: An Investigation of the Postoperative Brain-Tumor Interface.* Int J Radiat Oncol Biol Phys, 2010: p. 1-6.

95.   Sadzuka, Y., R. Hirama, and T. Sonobe, *Effects of intraperitoneal administration of liposomes and methods of preparing liposomes for local therapy.* Toxicol Lett, 2002. **126**(2): p. 83-90.

96.   Pradhan, P., et al., *Targeted temperature sensitive magnetic liposomes for thermo-chemotherapy.* J Control Release, 2009: p. (14pp).

97.   Lindner, V. and H. Heinle, *Binding properties of circulating Evans blue in rabbits as determined by disc electrophoresis.* Atherosclerosis, 1982. **43**(2-3): p. 417-22.

98.   Hueper, W.C. and C. Ichniowski, *Toxicopathologic Studies on the Dye T-1824.* AMA Arch Surg, 1944. **48**(1): p. 17.

99.   Roberts, L.N., *Evans blue toxicity.* Can Med Assoc J, 1954. **71**(5): p. 489-91.

100.   Bolotin, E.M., et al., *Ammonium Sulfate Gradients for Efficient and Stable Remote Loading of Amphipathic Weak Bases into Liposomes and Ligandoliposomes.* Journal of liposome research, 1994. **4**(1): p. 455-479.

101.   Ghaghada, K.B., et al., *New dual mode gadolinium nanoparticle contrast agent for magnetic resonance imaging.* PLoS One, 2009. **4**(10): p. e7628.